Space Sci Rev
DOI 10.1007/s11214-008-9383-7

Cross Sections and Reaction Rates for Comparative Planetary Aeronomy

David L. Huestis · Stephen W. Bougher · Jane L. Fox · Marina Galand · Robert E. Johnson · Julianne I. Moses · Juliet C. Pickering

Received: 29 January 2008 / Accepted: 21 May 2008

Abstract In this chapter we describe the current knowledge of a selection of collision processes and chemical reactions of importance to planetary aeronomy. Emphasis is placed on critical evaluation of what we know and what we wish we knew about fundamental processes required for interpretation, explanation, and modeling of atmospheric observations.

Keywords Collisions · Photoabsorption · Chemical reactions · Critical evaluation · Laboratory measurement · First-principles theory · Needs in atmospheric models

1 Introduction, Objectives, and Outline

In this chapter we highlight some of the optical, chemical, and collisional processes involving atoms and molecules of importance in the upper atmospheres, ionospheres, and magne-

Prepared for publication in Space Science Reviews (Springer) and in the International Space Science Institute (ISSI Bern) book series, Volume 29.

D.L. Huestis (✉)
Molecular Physics Laboratory, SRI International, Menlo Park, CA 94025, USA
e-mail: david.huestis@sri.com

S.W. Bougher
Atmospheric, Oceanic and Space Sciences, University of Michigan, Ann Arbor, MI 48109, USA

J.L. Fox
Department of Physics, Wright State University, Dayton, OH 45435, USA

M. Galand · J.C. Pickering
Space and Atmospheric Physics, Imperial College London, London, SW7 2AZ, UK

R.E. Johnson
Engineering Physics and Materials Science, University of Virginia, Charlottesville, VA 22904, USA

J.I. Moses
Planetary Science, Lunar and Planetary Institute, Houston, TX 77058, USA

tospheres of the planets, moons, and comets in the solar system. The atmospheric domain extends roughly from the lowest altitudes at which dissociation and ionization are important, through the corona and into the ambient plasma where ion-neutral collisions are important. The range of chemical species extends from photons, electrons, and protons, through moderate molecular-weight organic molecules. The collision energies range from several meV, corresponding to the local temperature, up to 100's of keV, appropriate for particles in the solar wind and planetary magnetospheres.

As a companion with the other chapters in this volume, the discussion here must necessarily be selective, emphasizing processes that are important in more than one atmosphere, or at least are similar to those in other atmospheres. The limitations of space imply that we can include only a very small fraction of the microscopic chemical and collisional processes that are included in current atmospheric chemistry models. The obvious bias is for processes that are "important." In addition, we emphasize processes that are currently not well quantified, have been a topic of recent controversy, or have been the subject of recent experimental or theoretical investigations.

The optical, chemical, and collision processes to be addressed are divided into the following seven categories:

1. Chemical reactions of neutral atoms and molecules in their ground electronic states
2. Ion–molecule reactions
3. Chemistry, relaxation, and radiation of electronically excited atoms and molecules
4. Vibrational and rotational excitation, relaxation, and radiative emission
5. Photoabsorption, photodissociation, and photoionization
6. Electron-impact excitation, dissociation, ionization, and recombination
7. Energetic heavy particle excitation and charge exchange

Below we will briefly review how cross sections and reaction rates are used in data interpretation and modeling. The main component of this chapter is a limited critical evaluation of a few processes in each of the seven categories listed above. We will conclude with an extensive list of cited references, highlighting key laboratory measurements, first-principles calculations, the atmospheric models in which they are incorporated, and the atmospheric observations they help to characterize and explain.

2 Fundamental Processes in Planetary Atmospheres

In this section we will provide several examples of how cross sections and reaction rates are used in observational data interpretation and modeling, by atmospheric type, region, event, or observable. The key is in identifying what is important and what we wish we knew.

2.1 Inner Planets

The recent Mars and Venus Express missions have stimulated renewed interest in comparative investigations of the atmospheres of the Earth and its near neighbors. In this Section we will review interconnections between microscopic collisional processes, atmospheric motion, thermal balance, and remotely observable signatures.

2.1.1 Nightglow

Direct wind measurements of the Venus and Mars upper atmospheres are currently lacking. Such wind retrievals, in conjunction with simultaneous density and temperature measurements, would provide a means to constrain General Circulation Models (GCMs) and

thereby characterize the self-consistent thermal, wind, and compositional structure of these upper atmospheres over solar cycle, seasonal, and diurnal timescales. This ideal situation is presently far from being realized in our study of the Venus and Mars upper atmospheres (e.g. Bougher et al. 1997, 2006a, 2006b).

Instead, creative application of available nightglow observations at both Venus and Mars, in conjunction with GCMs, is being used to infer global circulation patterns, wind magnitudes, and their variations over solar cycle and seasonal timescales (e.g. Bougher et al. 1990, 1997, 2006a, 2006b; Bougher and Borucki 1994; Bertaux et al. 2005). At Venus, NO UV nightglow, $O_2(^1\Delta_g)$ 1.27-μm nightglow, and O_2 400–800 nm nightglow intensity distributions and their temporal variability are being used to constrain GCMs and uncover the thermospheric general circulation patterns and wind magnitude responsible. Pioneer Venus, Venus Express, and ground based nightglow observations have all contributed to this process of tracing Venus thermospheric wind patterns (see reviews by Lellouch et al. 1997; Bougher et al. 1997, 2006a; Gerard et al. 2008). At Mars, recent Mars Express SPICAM observations of NO nightglow emissions at high latitudes (Bertaux et al. 2005) plus several winter polar warming measurements from aerobraking missions (e.g. Bougher et al. 2006b) are motivating new GCM simulations that seek to determine the seasonal and solar cycle variations in the Mars thermospheric circulation.

The effectiveness of these nightglow studies to constrain the Venus and Mars thermospheric circulation patterns is predicated upon a firm understanding of the physical processes responsible for the creation of the nightglow emission features. A few key reactions and rates are poorly constrained, leading to ambiguity in nightglow calculations for comparison to observations. Specifically, 3-body recombination ($O+O+CO_2$) is assumed to be the major contributor to the production of the $O_2(a^1\Delta_g)$ state and the observed Venus 1.27-μm nightglow emission. Quenching of this $O_2(a^1\Delta_g)$ state, notably by CO_2, competes with this production. Firm measurements of this 3-body reaction rate (and ~100–250 K temperature dependence) and the corresponding CO_2 quenching rate are needed to refine these nightglow calculations within model simulations. Furthermore, the effective yield of the $O_2(a^1\Delta_g)$ state from 3-body recombination is assumed to be ~0.75–1.0 (e.g. Gerard et al. 2008). A measurement of the absolute value of this yield in CO_2 is also greatly needed to further constrain model simulations. The interpretation of recent Venus Express $O_2(^1\Delta_g)$ 1.27-μm nightglow distributions (Gerard et al. 2008) will be greatly advanced by such new laboratory measurements.

See also Slanger et al. (2008b) in this Volume and Sects. 3.1.2 and 3.3.2 of this chapter.

2.1.2 O–CO_2 Cooling

The role of CO_2 15-μm cooling in the thermospheric heat budgets of Venus, Earth, and Mars is described to be profoundly different (see reviews by Bougher et al. 1999, 2000, 2002). However, a self-consistent and definitive treatment of these differences requires the application of a realistic and common O–CO_2 vibrational re-excitation rate. This rate has recently been measured in the laboratory at room temperatures and found to be $\sim 1.5 \times 10^{-12}$ cm^3/sec (see Khvorostovskaya et al. 2002; Akmaev 2003; Sect. 3.4.2 of this chapter), in contrast to values of $\sim 3.0 \times 10^{-12}$ cm^3/sec (or larger) commonly used in recent GCM model simulations that seek to compare the heat budgets of Venus, Earth, and Mars using a common modeling framework (e.g. Bougher et al. 1999, 2000, 2002). This discrepancy may be due in part to uncertainties in the upper atmosphere atomic O abundances for Venus and Mars. In particular, O abundances have never been directly measured for the Mars upper atmosphere, only inferred from UV airglow measurements (e.g. Stewart et al. 1992;

Alexander et al. 1993) and ionospheric calculations (e.g. Hanson et al. 1977; Fox and Dalgarno 1979). Values should vary considerably over the solar cycle, seasons, and latitudes on Mars. A proper evaluation of the impacts of CO_2 15-μm cooling on the Mars thermosphere, even assuming the modern laboratory O–CO_2 vibrational re-excitation rate, must await new Martian in-situ composition measurements. Similarly, Venus atomic O abundances have been measured by the Pioneer Venus ONMS instrument near the equator above ∼135 km for solar maximum conditions (e.g. Niemann et al. 1979, 1980; Hedin et al. 1983). However, abundance measurements throughout the rest of the solar cycle and over wide latitude regions are missing.

In addition, our present understanding of both Venus and Mars thermospheric heat budgets is predicated upon detailed EUV-UV heating efficiency calculations conducted most recently for Venus (Fox 1988) and Mars (Fox et al. 1995). Efficiencies of $21 \pm 2\%$ are reasonable and should be applicable to the Mars thermosphere; profiles of 20–22% are acceptable for the Venus thermosphere. Uncertainties in these efficiencies, although small, still provide some flexibility when applying the recently measured O–CO_2 rate ($\sim 1.5 \times 10^{-12}$ cm^3/sec) in model calculations designed to reproduce measured temperatures and their variations over the solar cycle and seasons.

In short, CO_2 15-μm cooling rates and their impacts upon the Venus and Mars thermospheres are best quantified and compared once: (1) atomic O abundances are properly characterized for both planets, (2) an appropriate EUV-UV heating efficiency is assumed, and (3) a common (and modern) O–CO_2 vibrational re-excitation rate ($\sim 1.5 \times 10^{-12}$ cm^3/sec near 300 K) is applied. See also Sect. 3.4.2 in this chapter.

2.2 Outer Planets

Solar-radiation-driven photochemical processes are very important on the giant planets despite the relatively large distances of these planets from the Sun. In the uppermost portions of giant-planet atmospheres, extreme ultraviolet radiation and X-rays interact with hydrogen and other constituents, leading to photoionization (for reviews of ionospheric processes on the giant planets, see Witasse et al. (2008) in this issue, Nagy and Cravens (2002), and Majeed et al. (2004). The dominant primary ion, H_2^+, reacts quickly with H_2 to produce H_3^+ or charge exchanges with H to form H^+. Radiative recombination of H^+ is slow, so H^+ can become the dominant ion in giant-planet ionospheres, especially in regions where the daily average flux of solar radiation is highest (e.g., in the summer, at low latitudes, at solar maximum) and at night at all latitudes. The H_3^+ ions can dominate during the afternoon at middle and high latitudes (e.g. Moore et al. 2004), but dissociative recombination is fast enough that H_3^+ can recombine at night, and a significant diurnal variation of H_3^+ is expected.

Ion–molecule reactions are prevalent, especially in the lower ionosphere, where neutral hydrocarbons can interact with ions. Rate coefficients for ion–molecule reactions relevant to the giant planets (and Titan) have been reviewed by Anicich and McEwan (1997). Although the rate coefficients for the most important reactions are reasonably well known, the product distributions are less well known. In addition, the rate coefficients and products for important electron recombination reactions need further characterization. Interaction of charged particles from the magnetosphere also instigates upper-atmospheric chemistry on the giant planets, especially in the auroral regions (see Wong et al. 2000, 2003; Friedson et al. 2002), and many of the details (including rate coefficients, pathways, role of excited states, etc.) of this process remain to be worked out.

In the middle atmospheres of the giant planets, methane photolysis (primarily at Lyman alpha wavelengths) drives a complex hydrocarbon photochemistry that results in the production of species like CH_3, C_2H_2, C_2H_4, C_2H_6, C_3H_4, C_3H_8, C_4H_2, and C_6H_6, which have all

been observed on one or more of the giant planets. Details of hydrocarbon photochemistry on the giant planets can be found in Moses et al. (2004, 2005); Yung and DeMore (1999); and Gladstone et al. (1996). Many uncertainties in this hydrocarbon chemistry remain, largely due to a lack of relevant laboratory and theoretical data on photodissociation cross sections, photodissociation quantum yields and branching ratios, reaction rate coefficients, and reaction pathways at low temperatures and pressures. Although much progress in determining the photoabsorption cross sections at relevant temperatures has been made in recent years (e.g. Wu et al. 2001, 2004; Chen and Wu 2004; Fahr and Nayak 1994, 1996; Bénilan et al. 2000; Chen et al. 1991, 2000; Smith et al. 1991, 1998), critical information about the *photodissociation* cross sections and product yields is missing. One particularly relevant case in point is that for methane photolysis at Lyman alpha. Only in recent years have the primary products and H and H_2 quantum yields been well characterized (e.g. Cook et al. 2001; Wang et al. 2000; Smith and Raulin 1999; Brownsword et al. 1997; Heck et al. 1996; Mordaunt et al. 1993); however, the quantum yield of CH, which is of critical importance for the production of unsaturated hydrocarbons, is still uncertain. In addition, the branching ratios from photolysis of other major hydrocarbons (e.g., C_2H_2, C_2H_4, C_2H_6, CH_3C_2H, C_3H_8) need to be worked out in better detail.

Other critical missing information is the low-pressure limiting behavior and/or falloff-region rate coefficients for termolecular reactions at low temperatures that are relevant to giant-planet atmospheres. Much of the action in terms of hydrocarbon photochemistry occurs in the 0.001–10 mbar pressure region, and typical temperatures range from 80–170 K. Termolecular reactions are of great importance on the giant planets despite the low pressures involved. Given the prevalence of atomic hydrogen in the photochemically active regions, low-pressure rate coefficients for $H + C_2H_x$, $H + C_3H_x$, and $H + C_4H_x$ are particularly needed, as are the details of benzene production and loss under appropriate conditions for giant-planet stratospheres. In Table 6 of Moses et al. (2005), some specific chemical kinetics needs for giant-planet hydrocarbon photochemical modeling are described.

See also Sects. 3.1.1, 3.2.1, and 3.2.2 of this chapter.

2.3 Ionospheres

The non-auroral ionospheres of the Earth and planets are produced by photoionization and photoelectron impact ionization of thermospheric atoms and molecules.

2.3.1 Inner Planet Ionospheres

Earth, Venus and Mars all have oxidizing atmospheres, but the major constituents of the atmospheres are N_2 and O_2 for Earth, and CO_2 and N_2 for Venus and Mars. In all three atmospheres, there are small admixtures of the stable species Ar, He, and H_2, and small chemically unstable atomic and molecular radicals, such as O, NO, N, H, CO, and C, which are produced photochemically.

In the F_1 regions of these ionospheres, the ions are produced by absorption of solar EUV photons, whose wavelengths range from about 100 to 1000 Å. The major ions produced in this region, including CO_2^+ and N_2^+, and most of the minor ions are rarely the terminal ions. In the presence of sufficient densities of neutrals, ions whose parent neutrals are characterized by high ionization potentials (IP's) are transformed to ions whose parent neutrals are characterized by low IP's. Thus N_2^+ and CO_2^+ are transformed to O_2^+ and NO^+ by charge transfer and other ion-molecule reactions (cf. Fox 2002, 2006). The terminal ions in the

lower ionospheres of the terrestrial planets are O_2^+ and NO^+, which are destroyed mainly by dissociative recombination (DR), e.g.,

$$NO^+ + e \rightarrow N + O. \tag{1}$$

In fact, NO has the lowest IP (9.26 eV) among the major and minor thermospheric species; it is thus an important ion on all three planets, even in the absence of significant densities of NO. At higher altitudes, where the fractional ionization is large and neutral densities are small, the molecular ions produced by direct ionization and by photochemical processes may be destroyed by DR. Atomic ions, such as O^+, N^+, H^+, and C^+ cannot undergo DR, and radiative recombination, e.g.,

$$O^+ + e \rightarrow O + h\nu \tag{2}$$

is slow, with rate coefficients on the order of 10^{-12} cm^3/s (Escalante and Victor 1992; Slanger et al. 2004). As a result, the fractional ionization would be expected to increase indefinitely as the altitude increases, but eventually the major loss process becomes transport downward by ambipolar diffusion. Atomic ion density profiles thus form an F_2 peak at the altitude where the time constant for loss by chemistry is equal to that for loss by transport. On Earth, O^+ forms a prominent F_2 peak near 300 km. On Venus, the O^+ peak near 200 km is not as prominent, and is generally not visible in electron density profiles. On Mars, the Viking RPA data showed that the O^+ density peaks near 230 km, but it is everywhere less than that of the major ion, O_2^+ (e.g. Hanson et al. 1977). In the electron density profiles of the terrestrial planets, a secondary, but visible E-region peak is seen below the F_1 peak. This peak is formed from ionization by solar soft X-rays, with wavelengths in the interval ~10–100 Å, and by the concomitant high energy photoelectrons and secondary electrons. On earth, ionization of O_2 by solar Lyman β at 1026 Å is an additional source of the E-region peak (e.g., Bauer 1973).

2.3.2 Outer Planet Ionospheres

The outer planets, including Jupiter, Saturn, Uranus and Neptune, are composed primarily of H_2, He, and CH_4. There are also small atmospheric abundances of NH_3, C_2H_6, and C_2H_2 that vary among the four planets. The latter two species are formed by photochemical processes that originate ultimately from CH_4. Jupiter and Saturn also have small abundances of PH_3. Because ammonia condenses to form clouds in the middle atmospheres, NH_3 is not a major component of the thermospheres of any of the outer planets. PH_3 and large hydrocarbons may also be incorporated into aerosols and hazes. In the thermospheres, the densities of higher hydrocarbons fall off rapidly above the methane homopauses, and as a result above the upper thermospheres are composed of mostly of H_2, H and He.

In reducing atmospheres, where hydrogen is abundant, and neutral densities are large, ionization flows from ions whose (unprotonated) parent species have low proton affinities (PA's) to those whose parent neutrals have high PA's. Thus the principle ion produced in the main part of these atmospheres, H_2^+, is never the terminal ion; the PA of H is only 2.69 eV, while that of H_2 is 4.39 eV, and those of hydrocarbons are even larger. Thus the terminal major molecular ion in the F_1 region is predicted to be H_3^+, which is produced by reaction of H_2^+ with H_2, and the major atomic ion at the F_2 peaks is H^+. Modelers have, however, encountered difficulty in fitting the model electron density profiles, for which the F_2 peak density is about 10^6 cm^{-3}, compared to the smaller measured electron density peak of about 10^5 cm^{-3}, without postulating some chemical loss process for H^+, such as charge transfer

of H^+ to vibrationally excited H_2^+ (e.g., McElroy 1973; Cravens 1987). For Saturn, influx of water (PA = 7.24 eV) from the rings has been postulated to reduce the H^+ densities (Waite et al. 1997; Moore et al. 2006).

However, Kim and Fox (1994) showed that solar radiation in the wings of the H_2 absorption lines penetrates to the Jovian hydrocarbon layer, producing one or more layers of hydrocarbon ions that peak in the altitude range 300–400 km above the ammonia cloud tops near 0.6 bar. This is likely to be the case for Saturn as well, although it has not been modeled.

2.3.3 Ionospheres on Titan and Triton

The atmospheres of the satellites Titan and Triton are of intermediate oxidation state and are composed mostly of N_2, with small amounts of CH_4 and H_2 (e.g., Krasnopolsky and Cruikshank 1995; Yelle et al. 2006). The surface pressure (13.5 μbar vs. 1.5 bar) and temperature (∼38 vs. 94 K) are much lower on Triton than on Titan, and the major species on Triton condense at the surface. In the atmospheres of Triton and Titan, hydrocarbons may be produced ultimately from methane photochemically or by processes the follow the impact of energetic electrons from the magnetospheres of Neptune and Saturn, respectively. On Triton, however, hydrocarbons seem to be formed mostly below the ionospheric peak, while on Titan, production of higher hydrocarbons takes place below the methane homopause, which has been found by the Cassini Huygens probe to be unexpectedly high in the thermosphere (e.g., Strobel and Summers 1995; Yelle et al. 2006).

Predictions for the composition of the ionospheres of the two satellites thus differ substantially. On Titan the major ion was predicted and found to be $HCNH^+$, with large quantitites of hydrocarbon ions, such as $C_2H_5^+$, CH_3^+, CH_5^+, $C_3H_5^+$, and $C_4H_3^+$, and nitrile ions, $C_nN_kH_m^+$ (e.g. Fox and Yelle 1997; Keller et al. 1998; Cravens et al. 2006; Vuitton et al. 2007). N_2^+ (IP = 15.58 eV, PA = 5.13) is the dominant ion formed at high altitudes, but it is transformed photochemically in regions of sufficient neutral densities to species with either lower IP's, such as CH_4^+ ($IP_{CH_4} = 12.51$ eV) or those with higher PA's, such as CH_5^+ ($PA_{CH_4} = 5.72$ eV) and $HCNH^+$ ($PA_{HCN} = 7.46$ eV). The transformation of protonated hydrocarbon and nitrile ions on Titan continues, as in reducing atmospheres, from species whose parent (unprotonated) neutrals are characterized by low PA's to those whose parent neutrals have higher PA's.

On Triton, the ionosphere was found by the Voyager RSS to be quite robust (Tyler et al. 1989), with a maximum ion density near 350 km of (2.6–4.3) $\times 10^4$ cm^{-3}, and a secondary peak near 100 km with a density of about 3000 cm^{-3}. The major ion is predicted by most models to be C^+ ($IP_C = 11.3$ eV) (e.g. Lyons et al. 1992; Krasnopolsky and Cruikshank 1995; Strobel and Summers 1995), although N^+ ($IP_N = 14.5$ eV) was suggested by early models (e.g. Majeed et al. 1990). The ionosphere thus consists primarily of an F_2 peak, although the secondary peak may be an F_1 or E peak, depending on its formation mechanisms. The details of chemistry of C and C^+ are currently, however, uncertain (in both reducing and oxidizing atmospheres) and measurements of rate coefficients are needed for reactions involving both species such as charge transfer from N_2^+, N^+, O^+, and O_2^+ to C.

2.3.4 Ionosphere Summary

For all the planets, the data required to model these ionospheres include photoabsorption, photoionization, and photodissociation cross sections; the cross sections for interaction of solar photoelectrons with atmospheric gases; the rate coefficients for ion–molecule reactions that transform the ions, and the diffusion coefficients for ions and minor neutrals.

Little information is available on the diffusion coefficients for metastable species, such as $O(^1D)$ and $O(^1S)$. Of particular interest are the rate coefficients for charge transfer of atomic ions to atoms. The reactions of He^+ and O^{++} with molecules may result in fragmentation and the product branching ratios are often unknown. Significant progress has been make in determining the chemistry of the important metastable species $O(^1D)$, $O(^1S)$, $O^+(^2D)$, $O^+(^2P)$, and $N_2(A^3\Sigma_u^+)$, but their sources and sinks are not currently as well known as those of stable species.

For the reducing atmospheres, the rate coefficients for many reactions of hydrocarbons and their ions are unknown. Although it is doubtful that the chemistry of C_3 or higher hydrocarbons and their ions will be completely understood, some progress can certainly be made for the smaller species.

See also Sects. 3.2.1, 3.2.2, 3.3.1, 3.6.1, and 3.7.1 of this chapter.

2.4 Aurora

Energetic particle precipitation in auroral regions is an important energy source upon a planetary atmosphere. It affects the atmospheric composition and dynamics, the thermal structure and the electrodynamical properties of the upper atmosphere. Auroral emissions observed from ground-based and Earth-orbiting observatories and from space probes offer us an extremely valuable remote-sensing of the auroral particle source. Its quantitative analysis allows the identification of the type of precipitating particles and the assessment of the incident particle characteristics in terms of mean energy and energy flux (e.g., Galand and Chakrabarti 2002; Fox et al. 2008; Slanger et al. 2008b).

Assessing the response of an upper atmosphere to auroral particles and analyzing auroral emissions quantitatively require comprehensive modelling tools, describing the transport of these energetic particles in an atmosphere. One of the key inputs of such tools is the collision cross section set between the energetic particles—electrons, ions, or neutrals—and the atmospheric species (e.g., H_2, H, He, CO_2, CO, CH_4, N_2, N, O_2, O). The type of collisions includes ionization, dissociation, and excitation of the neutral species, as well as scattering and excitation of the energetic particles and charge-changing collisions in the case of energetic ions or neutrals. The auroral particle energies extend to larger values than that of the photoelectrons, reaching a few tens of keV in the auroral regions at Earth, up to a few tens of MeV at Jupiter. The minimum energy to consider for describing the transport of auroral particles in a planetary atmosphere is the ionospheric thermal energy for electrons ($\sim$0.1 eV) and the minimum collision threshold energy for ions and neutrals when cross section data are available. The assessment of physical quantities from auroral analysis is significantly limited by the uncertainties in impact cross sections. For illustration, the energy flux and mean energy of the incident particles derived from auroral emission analysis are changed by up to 16% and 23%, respectively, for 10-keV incident electrons, as a result of the mere use of different N_2 ionization cross section sets (Germany et al. 2001).

Apart from the particle impact cross sections, reaction rates are also required for analyzing the auroral emissions which are associated with excited states produced or lost through chemical reactions, such as the OI 630.0 nm red line (e.g., Lummerzheim et al. 2001) and the OI 557.7 nm green line (e.g., Jones et al. 2006). Photo-absorption cross sections are needed when the auroral emissions undergo 'true' absorption by atmospheric neutrals. This is the case of the following emissions widely used in auroral particle diagnostic: N_2 Lyman-Birge-Hopfield (LBH) band emissions partially absorbed by O_2 in the terrestrial atmosphere (e.g. Galand and Lummerzheim 2004) and H_2 Lyman and Werner band emissions partially absorbed by the hydrocarbon layer at Jupiter (e.g. Régo et al. 1999). Finally, in addition to

photo-absorption cross sections, scattering cross sections (e.g., resonance) are required when the auroral photons experience significant scattering in the atmosphere. Radiative transfer needs to be taken into account for modeling the OI 130.4 nm resonant triplet in the Earth's auroral regions (e.g. Gladstone 1992) and the H Lyman α spectral profile at the giant planets (e.g. Régo et al. 1999).

Thanks to recent laboratory measurements or theoretical derivations, more accurate cross section sets, such as electron impact ionization cross sections of N_2 (Shemansky and Liu 2005) and CH_4 (Liu and Shemansky 2006), excitation cross sections associated with N_2 LBH band emissions (Johnson et al. 2005), excitation cross sections of O_2 (Kanik et al. 2003; Jones et al. 2006) and proton charge-transfer cross section with O (Pandey et al. 2007), are now available. They will help towards more reliable auroral transport modelling results at planets and moons in the Solar System, with possible implication on auroral diagnostic (e.g., Johnson et al. 2005). An illustration of recent progress in auroral physics, made possible thanks to the availability of new cross section data, is proposed by Kharchenko et al. (2006). They used new S^{q+} and updated O^{q+} cross sections for a more reliable modeling of the X-ray spectra induced by precipitating oxygen and sulfur ions. The satisfactory agreement obtained by these authors between the modeled and observed X-ray spectra in the auroral regions of Jupiter provides a reconciliation between both datasets. It also allows the identification of the types of precipitating particles—an equal mixture of oxygen and sulfur ions—and an estimation of their energies, which is consistent with a magnetospheric origin and acceleration processes up to a few MeV/amu.

Despite the new cross sections made available the past years, there is still a true need for additional measurements or modelling due to lack of data or dataset with too restricted energy coverage, too large uncertainness or too low spectral resolution (e.g., Lindsay and Stebbings 2005; Galand and Chakrabarti 2006; Karwasz et al. 2006). Finally, the applicability of measurements obtained under laboratory conditions to space environment should be borne in mind (Lindsay and Stebbings 2005).

2.5 Tenuous Atmospheres

On a planetary body with a significant atmosphere, the density decreases with increasing altitude until the atmospheric molecules move very large distances in ballistic trajectories and collisions between atmospheric species are improbable. This region of the atmosphere, called the corona or the exosphere, directly interacts with the space environment, as described by Johnson et al. (2008) and Ledvina et al. (2008). Similarly the 'airless' bodies, such as the Moon, Mercury, Saturn's main rings, Europa and many of the other large satellites have a nearly collisionless, gravitationally bound ambient gas forming a tenuous atmosphere. A fraction of the atoms and molecules in these atmospheres escape and enter the plasma environment. The escaping or gravitationally bound atoms and molecules can be ionized by photon and electron impact, the same processes which form the ionosphere. Because the interaction between the planetary corona and the ambient fields is complex, the principal problem has been lack of accurate the electron temperatures and densities rather than the lack of cross sections. In this region additional processes become important: charge exchange and knock-on collisions with the ions in the incident plasma, either the background solar wind or magnetospheric ions or the locally formed pick-up ions.

Since tenuous atmospheres are simulated by Monte Carlo models, the primary collision processes dominate so that one needs to know the ionization, charge exchange and angular differential cross sections. For most atomic ion-neutral collisions either data is available, there are good models for extrapolating data (Johnson 1990), or there are freeware

programs (e.g., the SRIM package, Ziegler 2008) to estimate the cross sections and the deflections produced. Having said that, detailed angular-differential cross section for elastic collisions between open-shell atoms have been calculated for only a few systems (e.g., O + O: Kharchenko et al. 2000; Tully and Johnson 2001). Such cross sections are critical in describing the escape depths (Johnson et al. 2008). If the collisions in the exobase region are molecular, it is inappropriate to use the hard-sphere approximation to derive the differential cross section from the known total cross section, because that method assumes isotropic scattering.

If one needs to know the emission spectra produced by an incident ion, much less data is available. For fast ions, ionization typically dominates dissociation and the production of secondary electrons has again been well studied. Also, the ambient electron flux and the secondary electrons produced typically dominate the emission spectra.

However, many of interesting tenuous atmospheres have a molecular component. Therefore, the locally produced pick-up ions can also be molecular, so that impacts of energetic ($\geq$10's of eV) molecular ions with molecules can be the dominant heating process for the corona (Michael and Johnson 2005). For fast atomic ions colliding with molecules, again the ionization, total charge exchange and the secondary electron production are either measured or can be estimated from good models. However, the angular differential cross sections and dissociation channels are known for only a limited number of collision pairs and over limited energy range.

For charge exchange by very fast ions, which is dominated by distant collisions, one can often use dissociation product energies obtained for electron impact ionization and the deflections are often small. However, this is not the case for lower energy ($\leq$1 keV/u) processes. Recent measurements for H^+ and O^+ on O_2 (Luna et al. 2005) and H^+ and N^+ on N_2 (Luna et al. 2003) have improved the situation at Europa and Titan for a limited range of ion energies. However, energetic atomic or molecular ion interactions with H_2O, SO_2, and CO_2 at Europa, SO_2 at Io, CH_4 at Titan, Triton and Pluto, CO_2 and CO at Mars, etc. are not well described and simulations have relied on simple classical collision cross sections (Johnson et al. 2002). The data base for relevant molecular ions colliding with molecules, a critical process in Titan's corona, is very limited, except at very low, quasi-thermal energies ($\leq$1 eV) where ion-molecule reaction expressions can be used, as discussed earlier. The incident ions not only produce hot electrons but can, by charge exchange or by knock-on collisions, produce energetic neutrals. Total and angular cross sections and product distributions for collisions of energetic (>10 eV) neutrals with molecules are essentially not readily available. Recently, collisions of a hot (>10 eV) N with N_2 were calculated (Tully and Johnson 2002, 2003).

See also Sects. 3.6.2 and 3.7.1 of this chapter.

3 Representative Optical, Chemical, and Collisional Processes

3.1 Chemical Reactions of Neutrals

3.1.1 Recombination of Methyl Radicals

Planetary emissions of the methyl radical were observed for the first time in 1998 on Saturn and Neptune by the ISO mission satellite (Bezard et al. 1998, 1999). Concentrations were derived for valuable comparisons to models. CH_3 is produced by VUV photolysis of CH_4 and is the key photochemical intermediate leading to complex organic molecules on

the giant planets and moons. Thus correct model predictions are required for the correct simulation of the photochemical synthesis. These observations form a very sensitive test of the mechanism, and as a reactive intermediate methyl is also a good marker for the transport parameterizations employed.

A very sensitive parameter controlling methyl concentrations is the loss process by recombination,

$$CH_3 + CH_3 + H_2 \rightarrow C_2H_6 + H_2 \tag{3}$$

which is also the main ethane formation step. At low upper atmosphere pressures, collisional deactivation of hot ethane intermediates by hydrogen bath gas is rate determining. Data is only available for temperatures above the 115–140 K needed, and only at much higher pressures. Extrapolation of existing rate expressions beyond their intended ranges gives differences of over two orders of magnitude (MacPherson et al. 1983, 1985; Slagle et al. 1988).

New theoretical master equation calculations were therefore performed, guided by the higher temperature pressure dependent rate constant data and theoretical calculations of transition state structures, to provide sound rate constants for this important reaction (Smith 2003). The results are intermediate to the prior extrapolations, and somewhat lower than used in recent model studies that match the methyl data (Lee et al. 2000; Moses et al. 2005). In regions of high H atom concentration, the

$$H + CH_3 \rightarrow CH_4 \tag{4}$$

recombination reaction is also important in determining methyl concentrations, so a similar calculation was performed for this step (Smith 2003).

These low pressure limit stabilization rate constants can increase rapidly at low temperatures, and for larger molecules any pressure dependence or falloff must also be considered. So it is important to determine the proper temperature dependence, and this often will need to be done theoretically because experimental results at low temperature and pressure are rare and difficult to obtain. Some other recombination reactions have small energy barriers but are still important, such as

$$H + C_2H_2 \leftrightarrow C_2H_3. \tag{5}$$

Tunneling has profound effects here for increasing low pressure and temperature rate constants orders of magnitude above normal expectations and extrapolations (Knyazev and Slagle 1996).

3.1.2 Three-Body Recombination of Oxygen Atoms

Dayside photoabsorption of solar ultraviolet (UV) radiation by molecular oxygen in the upper atmosphere of Earth, and by carbon dioxide in the upper atmospheres of Venus and Mars, results in production of atomic oxygen

$$O_2 + h\nu \rightarrow O + O \qquad \text{Earth} \tag{6}$$

$$CO_2 + h\nu \rightarrow O + CO \qquad \text{Venus and Mars} \tag{7}$$

that eventually undergoes three-body recombination (Huestis 2002)

$$O + O + M \rightarrow O_2(^5\Pi_g, A^3\Sigma_u^+, A'^3\Delta_u, c^1\Sigma_u^-, b^1\Sigma_g^+, a^1\Delta_g, X^3\Sigma_g^-) + M. \tag{8}$$

On all three planets, the competition between photodissociation, recombination, and diffusive vertical transport controls the transition between the homosphere and the heterosphere, and thus the atomic and molecular composition of the mesosphere and lower thermosphere. After transport to the nightside by planetary rotation or by high-altitude atmospheric winds, the chemical energy stored in O atoms is converted by three-body recombination into electronic, vibrational, and rotational energy, eventually appearing as ultraviolet, visible, and infrared nightglow emissions (250–1270 nm range), which have been the subject of many laboratory and interpretive investigations. Oxygen atom recombination is the only source for O_2 nightglow and the resulting emissions of electronically excited O_2 are key tracers for photochemical and wave activity near the mesopause. Moreover, O-atom recombination contributes significantly to the total thermospheric heating rate below about 100 km (Roble 1995). Knowledge of the temperature-dependent rate coefficient for recombination of atomic oxygen is thus essential for accurate modeling of the atmospheric composition and energetics. Equally important is a detailed understanding of the electronic states of O_2 produced in oxygen atom recombination, and of what can be learned from their nightglow emissions.

Until recently, the most modern measurement of the rate coefficient for O-atom three-body recombination was 35 years old (Campbell and Gray 1973). The most recent comprehensive review (Baulch et al. 1976) is also over 30 years old and shows that the absolute rate coefficients for recombination and the reverse process, collision-induced dissociation, as well as the dependence on temperature and collider, were poorly determined, in spite of the relatively narrow error bars reported in individual studies. The available information is illustrated in Fig. 1.

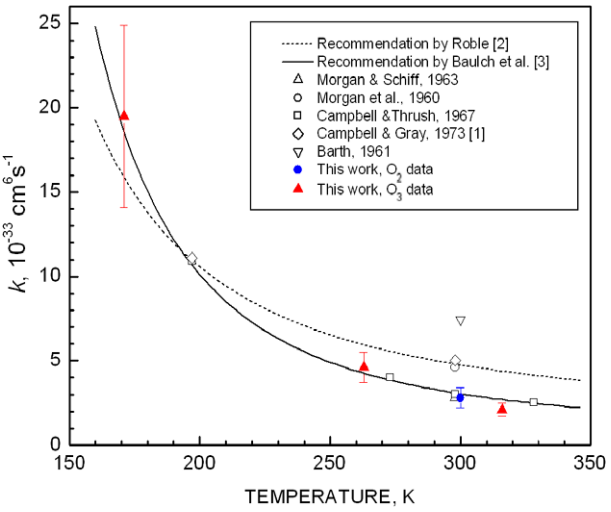

Fig. 1 Comparison of recommendations and measurements of the rate coefficient for oxygen atom three-body recombination in nitrogen. *Solid line*: recommendation by Baulch et al. (1976), adopted by the combustion modeling community. *Dashed line*: recommendation by Roble (1995), adopted by the atmospheric modeling community. *Open circle*: measurement by Morgan et al. (1960). *Open down triangle*: measurement by Barth (1961). *Open up triangle*: measurement by Morgan and Schiff (1963). *Open squares*: measurements by Campbell and Thrush (1967). *Open diamonds*: measurements by Campbell and Gray (1973). *Filled up triangles*: measurements using laser photodissociation of O_3 by Smith and Robertson (2008). *Filled circle*: measurement using laser photodissociation of O_2 by Pejaković et al. (2005, 2008)

Two recent laser-based experimental investigations have measured rate coefficients for O-atom three-body recombination in nitrogen (Pejaković et al. 2005, 2008; Smith and Robertson 2008). One experiment employed the pulsed output of a fluorine laser at 157.6 nm to achieve high degrees of photodissociation of molecular oxygen. In a high-pressure (1 atm) background of N_2, the produced oxygen atoms recombine in a time scale of several milliseconds. The O-atom population is monitored by two-photon laser-induced fluorescence at 845 nm, using a second laser with output near 226 nm. The measured value of the rate coefficient at room temperature is $(2.7 \pm 0.3) \times 10^{-33}$ cm^{6}s^{-1} (1-σ uncertainty), a value a factor of 2 lower than that currently adopted by the atmospheric modeling community. The second experiment employed a 248 nm KrF laser to achieve 100% photodissociation of molecular ozone. The time scale for O-atom recombination was followed by the same two-photon laser-induce-fluorescence technique. Recombination rate coefficients were measured at 170, 260, 300, and 315 K. The results of these two experiments are displayed in Fig. 1. These modern measurements are clearly consistent with the 30-year-old recommendations in use by the combustion modeling community (Baulch et al. 1976) and clearly inconsistent with the values favored by the atmospheric modeling community (Roble 1995).

The rate of recombination in CO_2 has not been measured, but has been estimated at 200 K to be about a factor of 2.5 faster than that in N_2 (Nair et al. 1994; Slanger et al. 2006). In both N_2 and CO_2 the overall yields of $O_2(a^1\Delta_g)$ and 1.27 μm radiation are believed to be close to unity, after accounting for collisional relaxation of the higher O_2 excited states produced initially by recombination (Huestis 2002; Slanger et al. 2006).

3.2 Ion Molecule Reactions

The diversity of the ionized molecules in planetary ionospheres was introduced above in Sects. 2.2 and 2.3 of this chapter. Correspondingly, complex sequences of chemical reaction transform the primary products of ionization by photon, electron, or heavy particle impact into the species that are eventually neutralized by recombination with electrons. In this section we review ion–molecule reactions that control the ionospheric electron density on the giant planets. Other important ion–molecule reactions are described in Sects. 3.3.1, 3.4.3, and 3.6.1 of the chapter. Also see the extensive collections of rate coefficients and recommendations by Anicich (2003).

3.2.1 $H_2^+ + H_2 \rightarrow H_3^+(v) + H$

H_3^+ made a surprise appearance in the very first molecular mass spectrum (Thompson 1911). Observation of M/Z of 3 instead of the expected M/Z of 2 is now understood as resulting from the fast reaction

$$H_2^+ + H_2 \rightarrow H_3^+(v) + H. \tag{9}$$

The H_3^+ laboratory infrared spectrum was first reported 69 years later (Oka 1980), observed in outer planet infrared aurorae about a decade thereafter (Drossart et al. 1989; Oka and Geballe 1990; Geballe et al. 1993; Trafton et al. 1993), and a widely used diagnostic of and initiator of isotopic and heavy-atom chemistry in interstellar clouds (Gerlich et al. 2002). The literature of experimental and theoretical investigations of the spectroscopy, electronic structure, potential energy surfaces, and chemical reactions of H_3^+ is far too vast for an adequate review here. Suffice it to say that H_3^+ is now better known than almost any other polyatomic molecule. Correspondingly, Reaction (9) is plausibly the most important ion–molecule reaction in outer planet ionospheres, and in the universe as a

whole. The rate coefficient is known. The product H_3^+ ion is known to contain vibrational energy, but the vibrational population distribution is currently unknown (Kim et al. 1974; Huestis and Bowman 2007; Huestis 2008).

3.2.2 $H^+ + H_2(v) \rightarrow H + H_2^+$ *or* $H^+ + H_2(v')$

The Pioneer and Voyager radio occultation experiments found electron densities in the ionospheres of the giant planets that were about an order of magnitude smaller than expected. Subsequent measurements from the Galileo and Cassini spacecraft have confirmed these observations. This has been one of the major puzzles in understanding planetary ionospheres.

The technical problem is illustrated by the following simple model:

$$H_2 + h\nu \rightarrow e + H_2^+ \text{ or } e + H^+ + H \tag{10}$$

$$H_2^+ + H_2 \rightarrow H_3^+ + H \quad \text{(fast)} \tag{11}$$

$$H_3^+ + e \rightarrow H_2 + H \text{ or } 3H \quad \text{(fast)} \tag{12}$$

$$H^+ + 2H_2 \rightarrow H_3^+ + H_2 \quad \text{(slow)} \tag{13}$$

$$H^+ + e \rightarrow H + h\nu \quad \text{(slow).} \tag{14}$$

Unless some new reaction is found to convert H^+ into H_2^+, H_3^+, or some other species that rapidly leads to electron–ion recombination, models predict that the protons (and thus the electrons) will reach greater densities than is consistent with observations.

As a result, modelers seized on the suggestion by McElroy (1973) that the endothermic charge transfer reaction

$$H^+ + H_2(v) \rightarrow H + H_2^+ \tag{15}$$

becomes exothermic for vibrational levels $v \geq 4$, and therefore might be expected to be fast. That point is illustrated in Fig. 2, which shows that the two asymptotic channels $H^+ + H_2$ and $H + H_2^+$ have the same energy at one value of the H_2 or H_2^+ internuclear distance, $R_{\text{vib}} \approx 2.5$ bohr or 1.32 Å. A number of modeling studies (Cravens 1974, 1987; Atreya et al. 1979; McConnell et al. 1982; Moses and Bass 2000; Hallett et al. 2004, 2005a, 2005b; Moore et al. 2004; Majeed et al. 2004) have followed the McElroy suggestion. Given a rate coefficient for Reaction (15), the key piece of missing information would be the H_2 vibrational distribution. A few studies explored reactions producing vibrationally excited hydrogen. Others used parameterized models of the vibrational distributions in the giant planet ionospheres, represented as altitude dependent rates for Reaction (15) or Reaction (14). Reaction (15) would be an important loss process for magnetic confinement fusion. A mitigating companion process is the vibrational relaxation reaction

$$H^+ + H_2(v_i) \rightarrow H^+ + H_2(v_f < v_i) \tag{16}$$

that had not been considered in previous ionospheric modeling studies.

We can use publications from the plasma fusion quantum theory community (Ichihara et al. 2000; Krstic 2002; Krstic et al. 2002; Krstic and Schultz 2003; Janev et al. 2003) to estimate rates of Reactions (15) and (16) at atmospheric temperatures (Huestis 2005b, 2008). Two studies (Ichihara et al. 2000; Krstic et al. 2002) investigated the charge transfer Reaction (15). By extrapolating to lower temperatures the results from the earlier study (Ichihara et al. 2000, Table 2) we estimate that Reaction (15) has a rate coefficient at 600 K

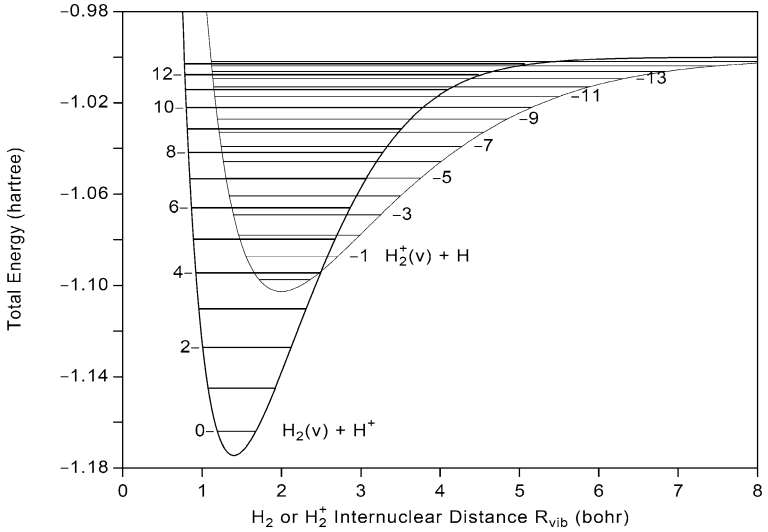

Fig. 2 H_2 and H_2^+ potential energy curves and vibrational energies

Table 1 Recommended rate coefficients at 600 K for $H^+ + H_2(v)$ charge transfer (k_{CT}) and vibrational relaxation (k_{VR}) in units of 10^{-9} cm^3/s

	v								
	0	1	2	3	4	5	6	7	8
k_{CT}	0	0	0	0	0.6	1.3	1.3	1.3	1.3
k_{VR}	0	1.2	1.8	1.8	1.5	1.2	1.2	1.2	1.2

of approximately 1.3×10^{-9} cm^3/s, for $v \geq 4$, consistent with numbers in current models. However, the later study (Krstic et al. 2002) (using more capable theory) found cross sections at thermal energies for $v = 4$ that are much smaller than those for $v \geq 5$. As a result of this disagreement, we have arbitrarily reduced the "recommended" rate coefficient for $v = 4$ shown in Table 1 by 50% compared to those for $v = 5$–8.

Another fusion-motivated investigation (Krstic 2002, Fig. 11) suggested that the vibrational relaxation Reaction (16) should be fast. From graphical analysis of this work we recommend thermal-energy rate coefficients of between 1.2×10^{-9} cm^3/s and 1.8×10^{-9} cm^3/s as indicated in Table 1. New quantum theory calculations are underway to reduce the uncertainties in these recommendations at low energy (Quemener et al. 2008).

Inclusion of Reaction (16) will significantly reduce calculated vibrational temperatures in ionospheric models. Protons are less abundant than neutral hydrogen atoms by a factor of about 10,000 and the proton rate coefficients for vibrational relaxation are about a factor of 10,000 larger. Just as important, Reaction (16) depletes excited vibrational population in vibrational levels 1, 2, and 3, which will contain the vast majority of vibrational energy for plausible vibrational distributions. The results of our earlier analysis (Huestis 2005b) have been adopted in a recent ionospheric modeling study (Moore et al. 2006), which suggests that the high influx of water indicated by Cassini observations will lead to a different mechanism for reducing the ionospheric electron density on Saturn (Connerney and Waite 1984;

Waite et al. 1997; Maurellis and Cravens 2001):

$$H^+ + H_2O \rightarrow H + H_2O^+. \quad (17)$$

3.3 Collisions of Excited Electronic States

3.3.1 Relaxation of $O^+(^2D)$ *and* $O^+(^2P)$ *in Collisions with* N_2 *and* $O(^3P)$

Atomic oxygen ions are primary charge carriers in the Earth's ionosphere. Optical emissions from the metastable excited states $O^+(^2D)$ and $O^+(^2P)$ provide useful diagnostics of energy deposition processes. The $O^+(^2P \rightarrow {}^2D,{}^4S)$ emissions near 732 and 247 nm are common features of the daytime and nighttime airglow. Previously, atmospheric $O^+(^2D \rightarrow {}^4S)$ emissions near 373 nm were known only during polar cusp aurorae (Sivjee 1983, 1991).

New observational information has been provided by recent analysis of sky spectra from the VLT (Very Large Telescope) in Chile during periods of large solar storms: 6–7 April 2000, 6–7 Nov. 2001, and 28 Oct.–1 Nov. 2003 (O'Neill et al. 2006; Slanger and Cosby 2007). $O^+(^2D \rightarrow {}^4S)$ 373 nm emissions are prominent and show a strong correlation with the Dst (disturbance storm time) index. Interpretation of the relative strengths of the $O^+(^2P \rightarrow {}^2D)$ 732 nm and $O^+(^2D \rightarrow {}^4S)$ 373 nm emissions requires reliable values for the rates of relaxation of the excited states in collisions with the principal components of the neutral ionosphere, N_2 and $O(^3P)$.

The current status of laboratory measurements and atmospheric modeling inferences is summarized in Table 2, along with recommended rate coefficients.

Of the four laboratory studies of charge-transfer, electronic-deexcitation, and ion-molecule reactions in collisions of $O^+(^4S,^2D,^2P)$ with N_2, only the most recent actually resolved the composition of the reactants, i.e., the relative abundance of $O^+(^4S)$, $O^+(^2D)$,

Table 2 Literature and recommended values of rate coefficients for collisional removal of $O^+(^2P)$ and $O^+(^2D)$, in units of 1.0×10^{-10} cm^3/s, taken from Huestis et al. (2007)

Reference	Method	$O^+(^2P) + N_2$	$O^+(^2P) + O(^3P)$	$O^+(^2D) + N_2$	$O^+(^2D) + O(^3P)$
WTH75	airglow	0.5 or 5	2 or 0		
RTH77	airglow	4.8	0.52		
GRT78	laboratory	1.5 ± 0.45[a]		1.5 ± 0.45[a]	
JB80a-b	laboratory	8 ± 2[a]		8 ± 2[a]	
RFF80	laboratory	8.3 ± 3.4[a]		8.3 ± 3.4[a]	
ATR84	N_2^+ model	4.8[b]	0.52[b]	8[b]	<0.05
CTR93	airglow	3.4 ± 1.5	4.0 ± 1.9		
LHF97	laboratory	2.0 ± 0.5		1.5 ± 0.4	
SMD03	airglow	1.8 ± 0.3	0.50 ± 0.34		
Recommendations		2.0 ± 0.5	0.4 ± 0.2	1.5 ± 0.4	0.6 ± 0.3

[a]Unknown mixture of $O^+(^2P) + O^+(^2D)$

[b]Values selected from works above

ATR84 = Abdou et al. 1984; CTR93 = Chang et al. 1993; GRT78 = Glosik et al. 1978; JB80a-b = Johnsen and Biondi 1980a, 1980b; LHF97 = Li et al. 1997; RFF80 = Rowe et al. 1980; RTH77 = Rusch et al. 1977; SMD03 = Stephan et al. 2003; WTK75 = Walker et al. 1975

and $O^+(^2P)$, as well as the identity of the product ion, e.g., N_2^+, NO^+, or N^+. The most recent laboratory and airglow modeling numbers agree for $O^+(^2P)$, providing strong support for each other and for the laboratory value for $O^+(^2D)$. There are no published laboratory or theoretical constraints for collisions with $O(^3P)$. The airglow modeling numbers similarly provide only very broad limits. Qualitative theoretical analysis (Huestis et al. 2007) based on the best-available O_2^+ potential energy curves by Beebe et al. (1976), suggests that we expect numbers around 5×10^{-11} cm^3/s for both $O^+(^2D)$ and $O^+(^2P)$, with the rate coefficient for $O^+(^2D)$ likely to be about twice as large as that for $O^+(^2P)$.

3.3.2 Rates and Products of Collisional Relaxation of $O_2(a^1\Delta_g)$ *and* $O_2(b^1\Sigma_g^+)$

The low-lying electronic excited states of molecular oxygen, $O_2(a^1\Delta_g)$ and $O_2(b^1\Sigma_g^+)$ are produced directly or indirectly after absorption of ultraviolet solar radiation in the atmospheres of Venus, Earth, and Mars. For example

$$O_3 + h\nu \rightarrow O(^1D) + O_2(a^1\Delta_g) \tag{18}$$

$$O(^1D) + O_2(X^3\Sigma_g^-) \rightarrow O(^3P) + O_2(b^1\Sigma_g^+) \tag{19}$$

$$O(^3P) + O(^3P) + M \rightarrow O_2(a^1\Delta_g) \quad \text{and} \quad O_2(b^1\Sigma_g^+). \tag{20}$$

At high altitudes, both $O_2(a^1\Delta_g)$ and $O_2(b^1\Sigma_g^+)$ are weakly quenched and produce strong airglow emission at 1270 nm (Venus, Earth, and Mars) and 762 nm (Earth), respectively.

At lower altitudes, oxygen molecules in either electronic state undergo collisional relaxation. The question to be addressed here is what can be said about the rates and products of this relaxation in the terrestrial atmosphere. More specifically, we wish to know how much of the electronic energy eventually ends up in vibrational excitation in $O_2(X^3\Sigma_g^-)$ which may contribute to observable infrared emission after vibrational energy transfer to H_2O or CO_2. A portion of the following analysis has already been published (Huestis 2005a). The reactions in question are

$$O_2(b^1\Sigma_g^+, v=0) + O_2(X^3\Sigma_g^-, v=0) \rightarrow O_2(X^3\Sigma_g^-, v') \text{ or } O_2(a^1\Delta_g, v') + O_2(X^3\Sigma_g^-, v'') \tag{21}$$

$$O_2(a^1\Delta_g, v=0) + O_2(X^3\Sigma_g^-, v=0) \rightarrow O_2(X^3\Sigma_g^-, v') + O_2(X^3\Sigma_g^-, v''). \tag{22}$$

While no direct measurements exist of the product distributions in either reaction, enough indirect information is available for construction of relatively reliable estimates.

Combining the data from low temperature (Seidl et al. 1991), room temperature (Sander et al. 2006), and high temperature shock tube studies (Borrell et al. 1979, 1982) we find that the temperature dependence of overall rate of electronic relaxation of $O_2(b^1\Sigma_g^+,\ v=0)$ in collisions with $^{16}O_2(X^3\Sigma_g^-,\ v=0)$ can be adequately represented from 90 to 1800 K by the formula

$$k_{21}(T) = 3 \times 10^{-18} + 4.5 \times 10^{-11} \exp(-91/T^{1/3}) \text{ cm}^3/\text{s}. \tag{23}$$

The form of this expression is a generalization of the Landau and Teller (1936) representation of vibrational and rotational relaxation (Huestis 2006a, 2008).

The overall rate of electronic relaxation of $O_2(a^1\Delta_g,\ v=0)$ in Reaction (22) has been measured near room temperature in a number of investigations (Sander et al. 2006), in liquid oxygen (Huestis et al. 1974; Protz and Maier 1980; Faltermeier et al. 1981; Klingshirn et al.

1982; Wild et al. 1982, 1984), and more recently in gaseous oxygen between 100 and 500 K (Billingham and Borrell 1986; Chatelet et al. 1986; Seidl et al. 1991). The gas phase data in normal oxygen can be represented adequately by the formula

$$k_{22}(T) = 0.14 \times 10^{-18} + 1.43 \times 10^{-18}\ (T/298). \tag{24}$$

Many investigators have reported high yields of $O_2(a^1\Delta_g)$ in Reaction (21) in the gas phase, including relaxation in collisions with H_2O, CO_2, and other collision partners (Singh and Setser 1985; Knickelbein et al. 1987; Wildt et al. 1988; Sander et al. 2006). Experiments performed in natural and isotopic liquid oxygen provide additional information about the resulting vibrational distribution (Klingshirn and Maier 1985). In natural liquid oxygen $O_2(b^1\Sigma_g^+)$ is quenched by $O_2(X^3\Sigma_g^-)$ with a rate coefficient of 5.5×10^{-18} cm^3/s, while in liquid $^{18}O_2$, the rate coefficient is only 3×10^{-19} cm^3/s. Subsequent experiments in low temperature gaseous oxygen also showed that $O_2(b^1\Sigma_g^+)$ is quenched about 10 times more slowly in $^{18}O_2$ (Seidl et al. 1991). The slower quenching in $^{18}O_2$ is interpreted as indicating that vibrational energy resonance is a critical factor, corresponding to the fact that the translational/rotational energy released in the reaction

$$O_2(b^1\Sigma_g^+, v=0) + O_2(X^3\Sigma_g^-, v=0) \rightarrow O_2(a^1\Delta_g, v') + O_2(X^3\Sigma_g^-, 3-v') \tag{25}$$

is about 150 cm^{-1} greater for $^{18}O_2$ than for $^{16}O_2$, implying that quenching of $O_2(b^1\Sigma_g^+)$ produces $O_2(a^1\Delta_g)$ plus three quanta of vibration. A similar discussion of vibrational energy resonance is used to explain why electronic relaxation of $O_2(b^1\Sigma_g^+,\ v=0)$ is so much faster at room temperature when the collider is N_2, producing $O_2(a^1\Delta_g, v=2) + N_2(v=1)$.

A similar argument applies for identification of the vibrational product distribution for relaxation of $O_2(a^1\Delta_g)$. Investigations in liquid $^{18}O_2$ showed much slower relaxation (Klingshirn et al. 1982; Wild et al. 1984; Seidl et al. 1991), with a rate coefficient of 2×10^{-21} cm^3/s compared to 1×10^{-18} cm^3/s in $^{16}O_2$. In low temperature gaseous oxygen, relaxation in $^{18}O_2$ is also slower by a similar factor (Seidl et al. 1991). This was explained by the observation that the translational/rotational energy released in the reaction

$$O_2(a^1\Delta_g) + O_2(X^3\Sigma_g^-) \rightarrow O_2(X^3\Sigma_g^-, v) + O_2(X^3\Sigma_g^-, 5-v) \tag{26}$$

is more than 400 cm^{-1} greater for $^{18}O_2$ than for $^{16}O_2$, implying that quenching of $O_2(a^1\Delta_g)$ produces $O_2(X^3\Sigma_g^-)$ plus five quanta of vibration. This conclusion is supported by one of the liquid oxygen studies (Wild et al. 1982) in which anti-Stokes Raman scattering was used to infer production of 3.8 ± 0.8 vibrational quanta in $O_2(X^3\Sigma_g^-, v)$.

3.4 Relaxation and Excitation of Rotational and Vibrational Levels

3.4.1 Vibrational Energy Transfer and Relaxation in O_2 *and* H_2O

Vibrational energy transfer from oxygen molecules to water molecules helps control the local temperature in the Earth's mesosphere through radiative cooling. Infrared emissions from water molecules provide remote diagnostics for the altitude profile of water. Modeling these emissions is made more complicated by the near degeneracy between the first excited vibrational levels of the water and oxygen molecules. The rate of vibrational energy exchange has been of interest to atmospheric scientists, combustion modelers, and developers

of chemical lasers. It has been recently inferred from analysis of unpublished laser-based laboratory experiments (Huestis 2006a). The reactions in question are

$$O_2(1) + O_2(0) \rightarrow O_2(0) + O_2(0) \tag{27}$$

$$O_2(1) + H_2O(000) \rightarrow O_2(0) + H_2O(000) \tag{28}$$

$$O_2(1) + H_2O(000) \leftrightarrow O_2(0) + H_2O(010) \tag{29}$$

$$H_2O(010) + H_2O(000) \rightarrow H_2O(000) + H_2O(000) \tag{30}$$

$$H_2O(010) + O_2(0) \rightarrow H_2O(000) + O_2(0). \tag{31}$$

The chemical kinetics and sound absorption literatures provide reliable values for the rates of Reactions (27) and (30) and strong evidence that Reactions (28) and (31) are slow in comparison with Reaction (29). Our analytical solution to the chemical reaction system above shows that the rate of Reaction (29) can only be measured with water mole fractions higher than 1%. The only measurement that satisfies this requirement is reported in a Ph.D. thesis (Diskin 1997) and a conference presentation (Diskin et al. 1996) from the combustion community. Reanalysis of that data yields our recommended value of $(5.5 \pm 0.4) \times 10^{-13}$ cm^3/s at 300 K, between the values favored by the atmospheric and laser modeling communities.

3.4.2 O–CO_2 *Cooling*

As indicated in Sect. 2.1.2 above, infrared emissions from bending-mode excited carbon dioxide, $CO_2(010)$, is a primary regulator of thermal balance in the atmospheres of Venus, Earth, and Mars. At higher altitudes the time scale for infrared fluorescence is shorter than the collisional excitation time. Oxygen atoms are expected to be the principle collision partner in the vibrational reexcitation. The rate coefficient remains a matter of some dispute, with laboratory experiments providing values that are factors of 2 or more lower than those preferred by some modelers. Here we will review the current status of laboratory experiments and theory, which the former continue to confirm the preference for rate coefficients in the low range.

The key reaction in question is

$$CO_2(v_2 = 0) + O(^3P_{J'}) \leftrightarrow CO_2(v_2 = 1) + O(^3P_J). \tag{32}$$

While the rate in the excitation direction, as written, is the key parameter for modeling atmospheric infrared emission, laboratory measurements are usually reported in the de-excitation or relaxation direction, which atmospheric scientists have also adopted for purposes of comparison.

The results from laboratory investigations at room temperature are summarized in Table 3, along with the summary recommendation provided here and adopted above in Sect. 2.1.2. The several diverse laboratory approaches are all returning mutually consistent rate coefficients for the presumed key reaction that are all well below the inferences of atmospheric modelers, which suggests that uncertainty in rate coefficient is not the critical issue. As discussed below, this conclusion is supported by theoretical studies and the experimentally observed temperature dependence.

Three rather old theoretical studies (Bass 1974; Schatz and Redmon 1981; Harvey 1982) of excitation of $CO_2(010)$ in collisions with oxygen atoms all ignored the fact that the open-shell $O(^3P)$ atom actually generated three electronic states, one of symmetry $^3A'$ and two of

Table 3 Laboratory measurements of the rate coefficient for relaxation of $CO_2(010)$ in collision with $O(^3P)$ at 300 K

Year	k (in units if 10^{-12} cm^3/sec)	Reference
1991	1.5 ± 0.5	Shved et al. 1991
1993	1.2 ± 0.2	Pollock et al. 1993
1994	0.5 ± 0.2	Lilenfeld 1994
2002	1.4 ± 0.2	Khvorostovskaya et al. 2002
2006	1.8 ± 0.3	Castle et al. 2006
2007	1.6 ± 0.2	Dodd et al. 2007
2008	1.5 ± 0.2	Recommendation, this work

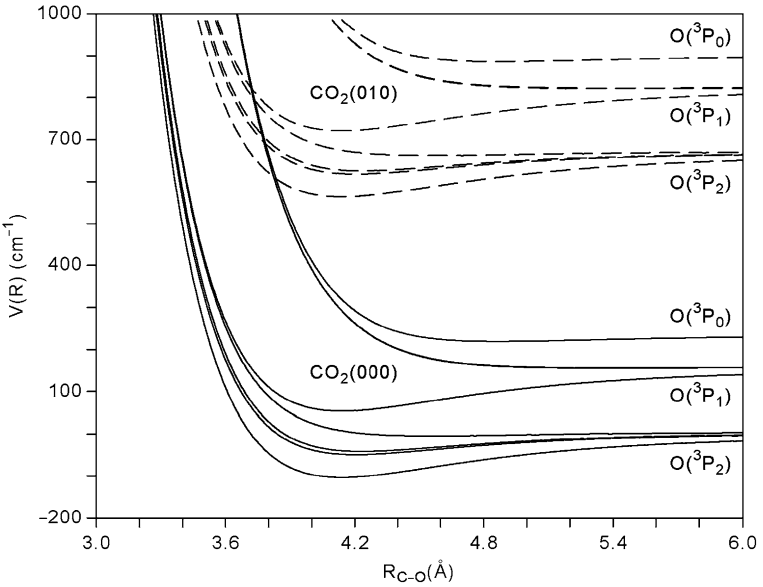

Fig. 3 Potential surfaces for $O(^3P) + CO_2(\nu_2 = 0)$, *solid lines*, and $O(^3P) + CO_2(\nu_2 = 1)$, *dashed lines*, with spin–orbit coupling, for 22.5° approach, from Huestis et al. (2002)

symmetry $^3A''$. Scott et al. (1993) provided the first curve-crossing model, following Nikitin and Umanski (1972), which enabled them to show that rate coefficients on the order of $1–2 \times 10^{-12}$ cm^3/s are indeed plausible.

Huestis et al. (2002) constructed the first set of model potential energy surfaces, including the three electronic states, calibrated by *ab initio* calculations. When spin–orbit coupling is included, a total of nine potential surfaces result, as shown in Fig. 3. The more recent calculations by de Lara-Castells et al. (2006, 2007) of $CO_2 + O(^3P)$, also included a representation of spin–orbit coupling. The two independent sets of potential energy surfaces provide strong support for the concept that the $O(^3P_J)$ fine structure states play critical roles in $CO_2(010)$ excitation and relaxation, as illustrated by the reaction

$$CO_2(000) + O(^3P_{0,1}) \leftrightarrow CO_2(010) + O(^3P_{1,2}) \tag{33}$$

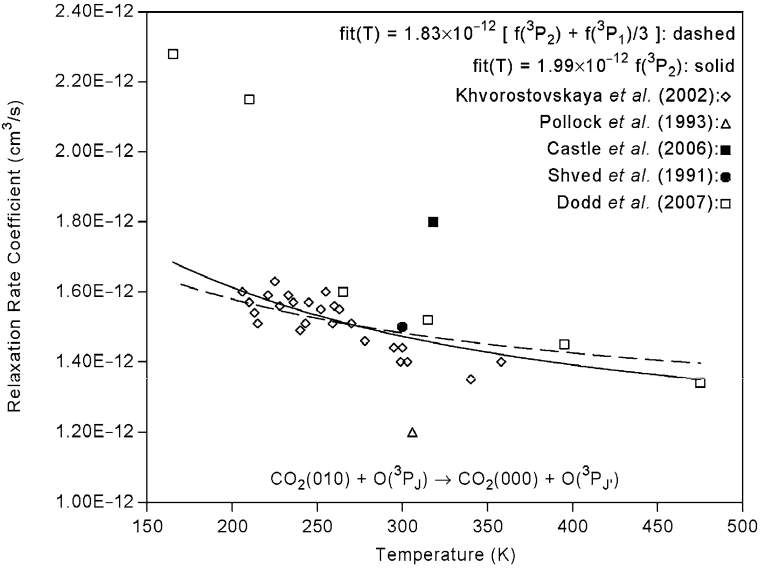

Fig. 4 Experimental rate coefficients and model fits for vibrational relaxation of $CO_2(010)$ in collisions with $O(^3P)$

which will be discussed further below. Comprehensive accurate chemical dynamics calculations have not been completed for this very complex system with four active atoms, nine active electronic states, and multiple potential surface crossings.

Additional theoretical guidance comes from the recent studies of vibrational relaxation at low temperature by Nikitin and Troe (Dashevskaya and Nikitin 2000; Dashevskaya et al. 2003, 2006, 2007; Nikitin and Troe 2006). They point out that quantum mechanics (Bethe 1937; Wigner 1948; Dashevskaya et al. 2003) implies the surprising conclusion that exoergic deexcitation reactions can have non-zero rate coefficients as the temperature approaches zero, in contrast to the normally expected $T^{1/2}$ dependence, as long as the interaction potential energy surface is attractive. They have verified this conclusion in accurate calculations of some simple vibrational relaxation collisions at low collision velocities (Dashevskaya et al. 2003).

Figure 3 shows that several of the potential surfaces arising from $CO_2(010) + O(^3P_{1,2})$ are attractive and intersect repulsive potential surfaces leading to curve-crossing deexcitation to $CO_2(000) + O(^3P_{0,1})$ at thermally accessible energies, even at low temperature. More detailed analysis of the potential surfaces in Fig. 3 suggests that all five of the potential surfaces arising from $O(^3P_2)$ and one arising from $O(^3P_1)$ are candidates.

Figure 4 shows the measured temperature-dependent $CO_2(010)$ deexcitation rate coefficients. The solid and dashed lines correspond to models in which we assume that the rate coefficient depends only on the temperature-dependent fraction of the oxygen atom population in the $O(^3P_2)$ and $O(^3P_1)$ spin–orbit sub-levels:

$$f(^3P_2) = 5/[5 + 3\exp(-225/T) + \exp(-326/T)] \tag{34}$$

$$f(^3P_1) = 3\exp(-225/T)/[5 + 3\exp(-225/T) + \exp(-326/T)]. \tag{35}$$

The quantitative adequacy of these simple models suggests that we are on the right conceptual track and that there is little reason to doubt the validity and accuracy of the labo-

ratory measurements. The single-measurement outlying values around room temperature, $(1.2 \pm 0.2) \times 10^{-12}$ cm^3/s (Pollock et al. 1993) and $(1.8 \pm 0.3) \times 10^{-12}$ cm^3/s (Castle et al. 2006) are both statistically consistent with the nominal value of $(1.5 \pm 0.2) \times 10^{-12}$ cm^3/s. The other two outlying values, at 165 and 210 K, from the most recent experiments of Dodd et al. (2007), might suggest a possible importance of long-range attraction due to interaction of the CO_2 vibrational dipole moment with the O-atom quadrupole moment. Given the atmospheric importance of this temperature range, and the divergence from the low temperature values from Khvorostovskaya et al. (2002), additional low temperature experiments are needed.

3.4.3 Vibrationally Excited H_3^+ in Outer Planet Atmospheres

The observed temperatures of planetary upper atmospheres, ionospheres, and thermospheres depend to a significant extent on the balance between absorption of ultraviolet solar radiation and infrared emission. On the outer planets the primary emitter is H_3^+ on the ν_2 vibrational fundamental and overtone transitions between 2 and 4 μm bands. At higher altitudes the low atmospheric densities imply that the reduced rates of collisional excitation of the emitting levels will eventually fall below the rates of spontaneous emission, thus limiting the efficiency of infrared emission. See Sect. 3.2.1 of the chapter above for additional discussion of production, ion–molecule reactions, and electron-ion recombination of atomic and molecular hydrogen ions.

The primary sources of vibrationally excited $H_3^+(v_2 > 0)$ are the H_3^+ formation reaction (Bowers et al. 1973; Theard and Huntress 1974; Kim et al. 1974) (note that the initial $H_3^+(v_2)$ vibrational distribution is only weakly constrained)

$$H_2^+ + H_2 \rightarrow H_3^+(v_2 > 0) + H \tag{36}$$

and $T \rightarrow V$ and $V \rightarrow V$ excitation in collisions with ambient H_2

$$H_3^+(v_2) + H_2(v) \rightarrow H_3^+(v_2') + H_2(v'). \tag{37}$$

Observations of H_3^+ emissions on Jupiter (Lellouch 2006) suggest that the $H_3^+(v_2)$ vibrational distribution is non-thermal and cooler than the ambient translational temperature as inferred from the observed $H_3^+(J)$ rotational distribution. Departures from local thermodynamic equilibrium (LTE) of H_3^+ population distributions are also observed in interstellar clouds (Oka and Epp 2004) and have been the subject of previous modeling studies of the Jovian ionosphere (McConnell and Majeed 1987; Kim et al. 1992; Miller et al. 2000, 2006; Grodent et al. 2001; Melin et al. 2005, 2006). In addition, the potential extent of vibrational excitation of H_3^+ is important in modeling gas discharges (Phelps 2001) and fusion plasmas (Janev et al. 2003), from which we can derive guidance for modeling the ionospheres of the outer planets.

Key missing pieces of information include the rate coefficients for redistribution of proton labeling and vibrational and rotational energy in the H_5^+ rearrangement collision

$$H_3^+(v_1, v_2, J, G) + H_2(v, J) \rightarrow H_5^+(v'', J'') \rightarrow H_3^+(v_1', v_2', J', G') + H_2(v', J'). \tag{38}$$

Characterizing this reaction experimentally is overwhelmingly difficult. The first challenge would be to prepare reactants with well-defined initial quantum numbers. The second challenge is measurement of the product quantum numbers. The third challenge is presented by the fact that each of the five protons in the H_5^+ reaction intermediate complex could have

come from either of the H_3^+ and H_2 reactants and could end up in either of the H_3^+ and H_2 products.

The third challenge could be considered an advantage if our actual interest were proton scrambling that leads to *ortho–para* conversion (Uy et al. 1997; Cordonnier et al. 2000; Oka 2004; Park and Light 2007). Alternatively, one could consider experiments and quantum theory calculations in which one or more of the H atoms are isotopically substituted by D atoms (Terao and Back 1969; Huntress and Anicich 1976; McMahon et al. 1976; Smith and Futrell 1976; Gerlich et al. 2002; Moyano and Collins 2003). In that case we have proton or deuteron transfer or more complicated rearrangement reactions such as

$$H_3^+ + D_2 \leftrightarrow (H_3D_2)^+ \leftrightarrow H_2 + HD_2^+ \text{ or } HD + H_2D^+ \tag{39}$$

$$D_3^3 + H_2 \leftrightarrow (H_2D_3)^+ \leftrightarrow D_2 + H_2D + \text{ or } HD^+HD_2^+ \tag{40}$$

$$H_3^+ + HD \leftrightarrow (H_4D)^+ \leftrightarrow H_2 + H_2D^+. \tag{41}$$

In these cases the differences between the zero-point vibrational energies means that the various product channels have different non-zero reaction exothermicities or endothermicities. In addition, proton and deuteron transfer reactions should have different rates because of the mass-dependent kinetic isotope effect. Furthermore, *ortho*/*para* selection rules and nuclear-spin degeneracies imply that the various entrance and exit channels may have different statistical weights. Finally, well-defined experiments would normally begin with vibrationally relaxed H_3^+ or D_3^+ reactants and thus would not provide direct information about vibrational deexcitation.

In spite of these complexities, isotopic substitution studies provide important information about the extent to which internal vibrational and rotational energy are statistically redistributed in formation and decomposition of the $H_5^+(v'', J'')$ reaction intermediate in Reaction (38). Stated in another way, can we use the probability of proton transfer (Janev et al. 2003) as a measure of rate of vibrational energy exchange, excitation, and deexcitation of H_3^+ with H_2 in Reaction (38)? In addition, Reactions (39)–(41) are important in their own right in modeling isotope fractionation in planetary ionospheres and interstellar clouds.

Table 4 contains a summary of the available kinetic information on isotopic forms of Reaction (38). As we can see from Table 4, the reported rate coefficients cluster into two groups:

(a) Small values in the range of 2.0–5.2 $\times 10^{-10}$ cm^3/s
(b) Large values in the range of 6.6–14.5 $\times 10^{-10}$ cm^3/s.

In some cases, numbers are reported that differ by more than a factor of three for the same reaction at the same temperature. The earlier room temperature experiments (Terao and Back 1969; Kim et al. 1974; Huntress and Anicich 1976; McMahon et al. 1976; Smith and Futrell 1976), the one 10 K experiment (Gerlich et al. 2002), and the very recent theoretical study (Park and Light 2007) of hyperfine spin scrambling are in the "small numbers" group, while the most comprehensive experiment (Giles et al. 1992) and theory (Moyano and Collins 2003) investigations are in the "large numbers" group.

As indicated by the divergences shown in Table 4, the current state of knowledge is most unsatisfactory. The factor-of-three scatter means that we have no plausible basis for an appropriate estimate for the rate coefficient for our target process, vibrational excitation and relaxation in Reaction (38). Further confusion comes from the fact that proton and deuteron exchange reactions should always lead to some V–V and V–T equilibration and thus could

Table 4 Summary of literature values of rate coefficients for selected $H_3^+ + H_2$ isotopomeric ion molecule reactions. Total reaction rate coefficients (to all products) are listed in units of 10^{-10} cm^3/s

Reaction						T (K)	Ref.	Note
(38)	(41)	(39)		(40)				
$H_3^+ + H_2$	$H_3^+ + HD$	$H_3^+ + D_2$	$H_2D^+ + HD$	$HD_2^+ + HD$	$D_3^+ + H_2$			
	3.5		2.6	2.0		10	GHR02	(a)
	12.1					10	MC03	(b)
0.0						10	PL07	(c)
4.9						10	PL07	(d)
	12.0	14.5	8.5	8.0	5.2	80	GAS92	(a)
	11.3	10.4				80	MC03	(b)
3.5						80	PL07	(c)
6.6						80	PL07	(d)
		3.3			3.3	300	TB69	(a)
2.7						300	KTH74	(e)
	3.0					300	HA76	(a)
			2.6	3.5		300	MMB76	(a)
					4.0	300	SF76	(a)
	9.6	12.6	5.0	4.5	8.2	300	GAS92	(a)

(a) Experiment
(b) Theory
(c) Theory: hyperfine scrambling for *para* H_2
(d) Theory: hyperfine scrambling for normal H_2
(e) Experiment: vibrational relaxation

GAS92 = Giles et al. 1992; GHR = Gerlich et al. 2002; HA76 = Huntress and Anicich 1976; MMB76 = McMahon et al. 1976; KTH74 = Kim et al. 1974; MC03 = Moyano and Collins 2003; PL07 = Park and Light 2007; SF76 = Smith and Futrell 1976; TB69 = Terao and Back 1969

be thought to provide lower limits for vibrational relaxation. In contrast, almost all the numbers in Table 4 are significantly larger than our most direct estimate for vibrational relaxation of $(2.7 \pm 0.6) \times 10^{-10}$ cm^3/s (Kim et al. 1974).

Thus we are left with the following unanswered science questions

- What is the mechanistic origin and cause of the sub-thermal vibrational distributions of H_3^+ (v_2) observed in the upper atmospheres of the outer planets?
- What are the key reactions and temperature-dependent rate coefficients that should be included in atmospheric models?
- What are the origin and resolution of the divergence between the "small values" and "large values" of the rate coefficients reported in the laboratory and quantum theory literature?

To answer these questions new theoretical investigations are planned for quantum electronic structure and chemical dynamics calculations for Reactions (36) and (38) (Xie et al. 2005; Huestis and Bowman 2007).

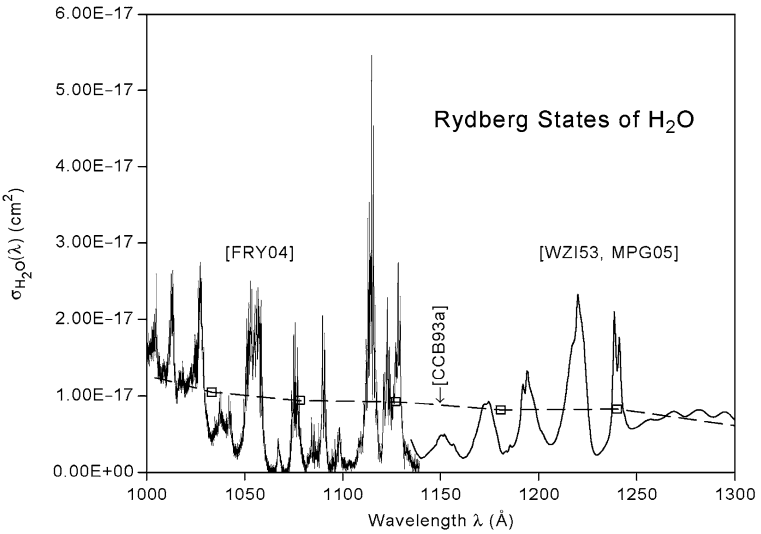

Fig. 5 A portion of the absorption cross section for water, H_2O, from Huestis and Berkowitz (2007). [CCB93a] = Chan et al. 1993; [FRY04] = Fillion et al. 2004; [MPG05] = R. Mota et al. 2005; [WZI63] = Watanabe et al. 1953

3.5 Photoabsorption

3.5.1 Absorption Cross Sections and Excited Photofragment Yields for CO_2 *and* H_2O

The Mariner flyby missions found strong ultraviolet emissions from CO_2^+(B,A), CO(a,A), and O(^{1}S) in the Mars dayglow. These observations, which have been confirmed by the recent Mars Express Mission, led to a number of laboratory quantum yield measurements.

Comet observers have supposed that the relative strengths of the O(^{1}S $\rightarrow$ ^{1}D) and O(^{1}D $\rightarrow$ ^{3}P) green (557.7 nm) and red (630.0 nm) lines can be used to infer the relative abundance of water and carbon dioxide in cometary coma (Delsemme 1980; Festou 1981; Festou and Feldman 1981; Huebner 1985; Cochran and Cochran 2001; Capria et al. 2005, 2008). Laboratory measurements have determined the yield of O(^{1}D) from photodissociation of water, but none of these experiments would have been capable of detecting O(^{1}S). In contrast, the wavelength dependent yield of O(^{1}S) from CO_2 has been investigated, but the yield of O(^{1}D) has been determined only at longer wavelengths, where the CO_2 absorption cross section is low (Huestis and Slanger 2006).

A portion of the water absorption spectrum is shown in Fig. 5.

For solar UV photodissociation Delsemme (1980) suggests yields of 12% for O(^{1}D) + H_2 and 1% for $O^* + H_2^*$ (other). On the other hand, Festou (1981) recommends 6.22% for O(^{1}D) + H_2 and 0.6% for O(^{1}S) + H_2. Interestingly, near Earth comets show a green/red ratio of about 0.1 (Cochran and Cochran 2001; Capria et al. 2005, 2008), hinting that Delsemme and Festou somehow got it right! What is actually known from previous laboratory experiments is the following:

Solar Lyman-α is by far the most important wavelength

$$H_2O + h\nu\ (\lambda < 242\ \text{nm}) \rightarrow OH(X^2\Pi) + H \qquad \text{known} \tag{42}$$

$$H_2O + h\nu\ (\lambda < 177\ \text{nm}) \rightarrow O(^1D) + H_2 \qquad \text{known} \tag{43}$$

$$H_2O + h\nu\ (\lambda < 136\ \text{nm}) \rightarrow OH(A^2\Sigma^+) + H \quad \text{known} \tag{44}$$

$$H_2O + h\nu\ (\lambda < 134\ \text{nm}) \rightarrow O(^1S) + H_2 \quad \text{unknown} \tag{45}$$

$$H_2O + h\nu\ (\lambda < 130\ \text{nm}) \rightarrow O(^3P) + H + H \quad \text{inferred.} \tag{46}$$

The yield of $O(^1D)$ was measured through its chemical reaction with H_2 or by 130 nm fluorescence scattering from $O(^3P)$, produced by relaxation in collisions with added N_2. No experiments performed to date would have been capable of identifying production of $O(^1S)$, a point made explicitly by Stief et al. (1975). McNesby et al. (1962) mention $O(^1S)$, not because it was detected, but only to show that it could not have been the source of observed OH fluorescence. Misinterpretation of this work is perhaps the source of Festou's estimate of the $O(^1S)$ yield.

A portion of the carbon dioxide absorption spectrum is shown in Fig. 6, along with a version of the solar UV spectrum, and the product of the two. Delsemme (1980) suggests yields from CO_2 67% for $O(^1D)$ and 22% for $CO^* + O^*$ (other). He never mentions $O(^1S)$, nor does he cite any of the papers reporting its production. He also does not cite the source of the high yield of $O(^1D)$. Similarly, Huebner (1985) presented an extensive table of photophysical processes (with no references to the primary literature), in which $O(^1S)$ is never mentioned as a CO_2 photodissociative product, in spite of the fact that in the same volume, Barth (1985) describes $O(^1S)$ production from CO_2 photodissociation at Mars. In fact, it was precisely the Mars observations (Barth et al. 1971) that led to the burst of quantum yield measurements in the 1970s.

The UV spectroscopy (Cossart-Magos et al. 1982, 1987) and absorption cross section (Nakata et al. 1965; Ogawa 1971; Slanger et al. 1974; Lewis and Carver 1983; Shaw et al. 1995; Yoshino et al. 1996; Berkowitz 2002; Huestis 2006b; Huestis and Slanger 2006; Stark et al. 2007; Huestis and Berkowitz 2007; Keller-Rudek and Moortgat 2008) of CO_2 have been extensively investigated. Several studies have determined the quantum yields for production of a wide variety of dissociation and ionization products, including $O(^3P)$ (Slanger and Black 1971; Zhu and Gordon 1990), $O(^1D)$ (Slanger and Black 1971; Zhu and Gordon 1990), $O(^1S)$ (Lawrence 1972; Ridley et al. 1973; Koyano et al. 1973; Slanger et al. 1977; Bibinov et al. 1979), as well as $CO(A^1\Pi)$, $CO(a^3\Pi$, and higher triplets), $CO_2^+(A^2\Pi$ and $B^2\Sigma^+)$, and $CO^+(B^2\Sigma^+)$. Astronomical observations or space missions motivated many of these studies. Okabe (1978) reviewed the earlier work. The data are not of uniform quality. There are wavelength gaps in the measured yields and neither the solar spectrum nor the absorption cross section is known with sufficient wavelength resolution.

Because of spin-conservation selection rules, it is widely believed (Schiff 1965; McElroy and Hunten 1970; Slanger and Black 1971, 1978; Slanger et al. 1974; Delsemme 1980; Zhu and Gordon 1990; Miller et al. 1992) that $O(^1D)$ is the primary product in the region from the energetic threshold at 7.5 eV up to the $O(^1S)$ threshold. However, there is little in the literature about direct detection of $O(^1D)$ at higher energy or shorter wavelength (Welge and Gilpin 1971). Thus we are unable to confirm the usual assumption that if the known quantum yield is less than unity, and if production of $O(^1D)$ is spin allowed, then it must have been the "dark" product. This uncertainty is important because the CO_2 absorption cross section is increasing rapidly at higher energy (shorter wavelength).

$O(^1S)$ is known to be produced from threshold at 9.6 eV (129 nm) to beyond the ionization limit at 13.8 eV (90 nm) (Lawrence 1972; Koyano et al. 1973; Slanger et al. 1977; Bibinov et al. 1979). In this spectral region, the absorption cross-section is quite strongly structured. Some absorption features are known to have unit yields of $O(^1S)$, while some others appear to produce purely $O(^1D)$. This variation has been difficult to quantify because

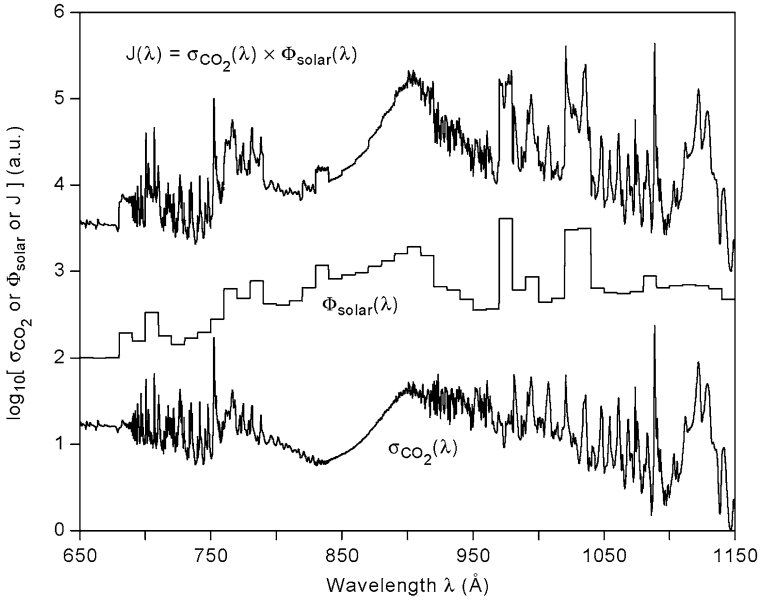

Fig. 6 Absorption cross section for carbon dioxide [σ_{CO_2}], the intensity of solar radiation [Φ_{solar}] and their product [J], from Huestis and Berkowitz (2007)

previous experiments generally used broadband light sources and made measurements at only a few widely spaced wavelengths.

The critical evaluation summarized here formed the basis for a new NASA-funded research program to measure the yields of $O(^1S)$ and $O(^1D)$ from photodissociation of H_2O and CO_2 using high spectral resolution VUV radiation from the Advanced Light Source at Lawrence Berkeley National Laboratory (Slanger et al. 2008a).

3.5.2 High Resolution Photoabsorption Cross Sections for SO_2

SO_2 is a known constituent of the atmosphere of Io (Ballester et al. 1994), but atmospheric studies of SO_2 using spectra acquired from the HST Faint Object Spectrograph (McGrath et al. 2000) have shown that the lack of laboratory measured high resolution cross sections limited the reliability of estimates of the SO_2 column density on Io. The use of low-resolution SO_2 data had led to the modelling of SO_2 ultraviolet (UV) absorption as a continuum when in reality it is a dense line spectrum. The spectrographs on board the current Venus Express also require high resolution cross sections for SO_2. It has been found that saturation of the very sharp SO_2 line features can lead to large underestimates of the SO_2 column density when instrumentally broadened absorption spectra are analyzed with low-resolution laboratory-derived cross sections (Stark et al. 1999). For very narrow spectral absorption features it is important to understand the difference between high- and low-resolution cross-section measurements (Hudson 1971). With inadequate instrumental resolution, measured cross sections at the centre of narrow absorption features are consistently underestimated and the cross sections in the "wing" regions between narrow features are consistently overestimated; the magnitude of the error being a function of the ratio of line width to instrument profile width, with the largest errors being associated with the lowest resolution. These systematic errors can be surprisingly large, as is seen in the case of SO_2 (see Fig. 7).

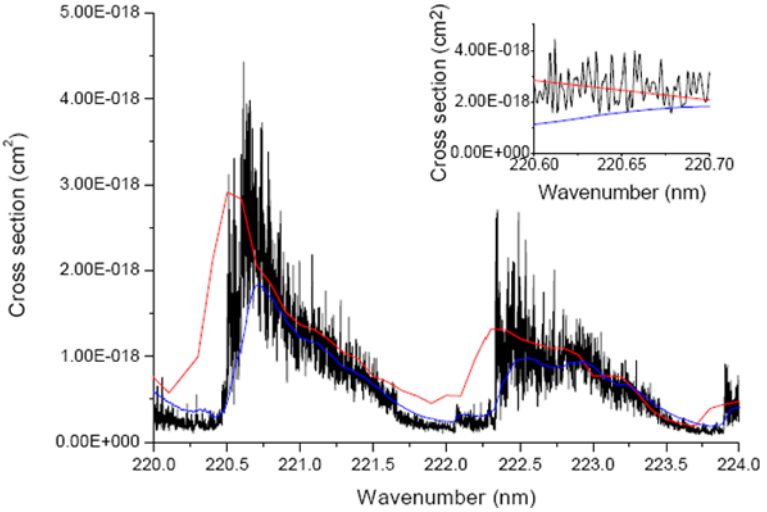

Fig. 7 Comparison of room temperature SO_2 absorption measurements (*4 nm segment, and inset 0.1 nm section*) carried out at different spectral resolution: high resolution 0.0004 nm (Rufus et al. 2003), low resolution compilation (0.1 nm) of Manatt and Lane (1993) (*red line*) and resolution 0.05 nm Wu et al. (2000) (*blue line*)

The UV spectrum of SO_2 has two main regions of significant absorption: a stronger absorbing region 175–230 nm, and a weaker region 250–320 nm. The spectrum is extremely complex at room temperature, and it is not possible to calculate the spectrum to sufficient accuracy for applications in planetary atmospheres (Stark et al. 1999). High resolution laboratory measurements of the SO_2 spectrum are required, and at a range of temperatures relevant to planetary atmospheres. Outlined here are the state-of-the-art measurements of high resolution photoabsorption cross sections undertaken at Imperial College in order to provide cross sections for SO_2 of sufficient accuracy for planetary atmosphere applications.

The basic components for experimental measurement of photoabsorption cross sections σ are: spectrometer, continuum light source, and absorption cell. The spectrometer used in this study was the Imperial College visible-UV Fourier Transform (FT) Spectrometer (Thorne et al. 1987), and resolving powers up to 550,000 were chosen to resolve the majority of the narrow SO_2 line features. The FT Spectrometer has advantages of high resolution, smoothly varying spectral response, linear wavenumber scale, and simultaneous observation of a wide spectral range. The continuum light sources were: a positive column hydrogen discharge, and high power deuterium lamp for the shorter wavelength region, and a 300 W xenon arc for the longer wavelength. The absorption cell contained 99.9% pure SO_2 with column densities ranging from 2.3×10^{16} cm^{-2} to 1.0×10^{19} cm^{-2} depending on the spectral region and range in σ magnitude. For each region several measurements at different pressures were made as checks to ensure that saturation effects were not present. The spectrum was measured in wavelength sections (10–20 nm bandwidth) by use of a novel zero-deviation zero-dispersion pre-monochromator, built at Imperial College (Murray 1992). This meant that good signal-to-noise ratio (SNR $>$ 50) could be achieved within a reasonable spectrum acquisition time (4–8 hours).

Commonly the experimental method involves recording the spectrum of a continuum source with (I_T) and without (I_o) the sample gas in the absorption cell. Although the continuum light sources are typically stable in intensity for an hour, over 8 hours, their

intensity has been observed to vary by a few percent. If the usual method of measurement with an empty gas cell, followed by filled cell, and a final empty cell, is used there will be errors in the resulting photoabsorption cross sections, as the continuum light source will have varied in intensity over the measurement time. For long acquisition times it was therefore essential to use the "dual beam technique". This makes use of the two outputs of the FT spectrometer (Rufus et al. 2003; Thorne et al. 1999; Davis et al. 2001). One output detector continuously measures the continuum light source, and the other measures the continuum light source with empty absorption cell, filled cell and then empty cell. Analysis of these spectra yields I_{o} and I_{T}, without errors arising from variations in the continuum light source.

However, care must be taken with choice of detectors. The response of photomultiplier tube detectors may also vary over the measurement timescales, and this variation can differ between detectors themselves. The photomultiplier detectors (Hamamatsu R166 and 1P28) were selected to be matched pairs from the manufacturer, and care was also taken to ensure their temperature remained constant during the day, again avoiding drifts in detector response. Wavelength calibration was carried out using iron standard lines (Learner and Thorne 1988), and wavelength accuracy is better than 10 mÅ.

Room temperature SO_2 measurements at Imperial College are completed (Stark et al. 1999; Rufus et al. 2003), and are the highest resolution SO_2 photoabsorption cross sections measurements undertaken to date. Uncertainties for σ in region 198–220 nm are estimated to vary from 10% for larger σ (10^{-17} cm^2) to 50% for lower σ ($<10^{-17}$ cm^2). In the longer wavelength region 220–325 nm uncertainties are typically 5% in regions of higher σ. In comparisons with previous photoabsorption cross section measurements in the literature (Rufus et al. 2003) there were differences in up to a factor of 2 in some cases arising in the main part from the resolution effect, and also shifts arising from wavelength errors. Figure 7 shows an example of the improvement in cross section data.

High resolution, low temperature, measurements are also required, to match atmospheric temperatures on Io and Venus. The Imperial College group, using the techniques described above, and a cooled gas cell, are undertaking measurements at 160 K in the range 190–220 nm, and at 200 K in the range 220–325 nm (Blackie et al. 2007). Some preliminary results are illustrated in Fig. 8.

These high resolution measurements over a range of temperatures have immediate applications in atmospheres where SO_2 is important, for example Io (Jessup et al. 2007). The use of low resolution laboratory photoabsorption cross sections leads to large errors in column densities estimates. Observations of planetary atmospheres with modern high resolution spectrographs require high resolution laboratory photoabsorption cross section data, at a range of temperatures, for full and reliable analysis.

3.6 Electron Collisions

As illustrated in previous sections of this chapter, electrons represent a primary source of excitation, dissociation, and ionization in planetary atmospheres and ionospheres. In addition, after thermalization in collisions with the ambient neutral atmosphere, electrons act like a chemical species, that is eventually consumed by dissociative recombination. Here we will review one specific case of dissociative recombination that contributes to atomic oxygen nightglow emissions. A second topic is creation of the atomic oxygen airglow on Europa and Ganymede by dissociative electron-impact excitation of molecular oxygen.

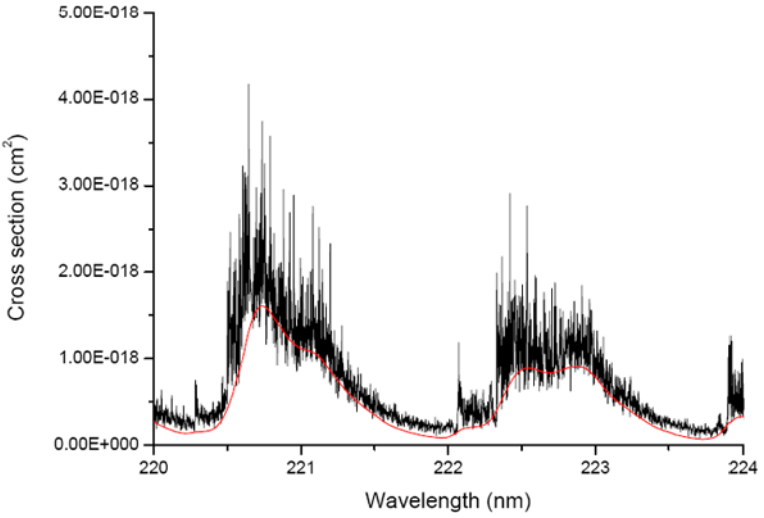

Fig. 8 Comparison of new high resolution 198 K temperature SO_2 photoabsorption cross sections (highly structured *black line*, Blackie et al. 2007) with the lower resolution results of Wu et al. (2000) (*red line*)

3.6.1 Dissociative Recombination of Electrons with Vibrationally Excited O_2^+

Dissociative recombination (DR) is the primary mechanism for electron loss in ionized, low-pressure molecular gases and plasmas, such as planetary ionospheres (Mitchell and Guberman 1989). Dissociative recombination occurs through a reaction written as

$$AB^+ + e \rightarrow A + B + \Delta E \tag{47}$$

for a diatomic molecular ion AB^+, atomic fragment products A and B, and kinetic energy release ΔE. Because the initial potential energy of the ion is usually 4 to 9 eV above the lowest dissociation limit of the neutral AB molecule, ample energy is available to leave some or all of the products A and B in electronically excited states (or in rotationally or vibrationally excited states if they are molecules instead of atoms). The excess energy ΔE appears as the center-of-mass kinetic energy given to the dissociation fragments. These two product characteristics, electronic excitation and high translation energy (which are connected by energy conservation), amplify the importance of dissociative recombination in the plasma by contributing to atmospheric heating (Torr et al. 1980; Fox 1988), planetary escape (Hunten 1982; Fox and Dalgarno 1983), optical emissions (Bates 1990), and the opening of new reaction channels in the ion and neutral chemistries.

The overall rates for dissociative recombination have been measured for many important species (Mitchell and Guberman 1989) and are generally considered to be reliably known, at least to within a factor of 2. Much less is known about the dependence of the rate on the initial vibrational state of the molecular ion, or about the branching ratios for production of specific excited states of the fragments. A previous study (Kella et al. 1997) of O_2^+ DR showed that vibrational excitation doubled the yield of $O(^1S)$. Although that experiment highlighted the effects of vibrational excitation, it offered no way of measuring the actual vibrational distribution. The expected influence of vibrational excitation on yields of atomic oxygen excited states is illustrated schematically in Fig. 9. With increasing vibrational excitation, the vibrational wavefunction is able to reach curve crossings between the initial

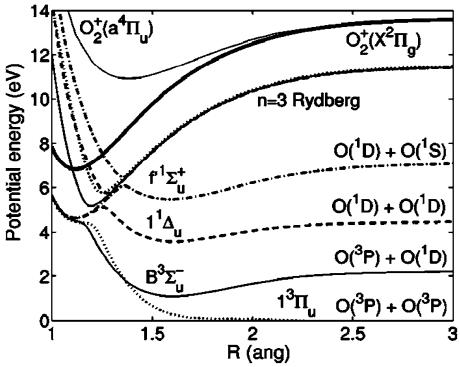

Fig. 9 Schematic potential curves relevant for the DR process with O_2^+, taken from Petrignani et al. (2005). The bound electronic ground $X^2\Pi_g$ and metastable excited $a^4\Pi_u$ states of the molecular ion are shown, along with the bound 3s Rydberg states of the neutral oxygen molecule (parallel to the $X^2\Pi_g$ ion state). The repulsive neutral electron-capture states, correlating with the various atomic asymptotes, illustrate the non-adiabatic interactions with the intermediate 3s Rydberg states

$O_2^+(X^2\Pi_g)$ potential curve and higher repulsive potential curves of neutral O_2 that correlate with more highly excited atomic fragments.

In the ionospheres of both Venus and Mars, O_2^+ is the most abundant molecular ion, followed by CO_2^+ and NO^+ (Hanson et al. 1977; Fox 2006). This result was initially surprising, given that there is relatively little O_2 in either atmosphere. O_2^+ is formed in two fast exothermic reactions:

$$O + CO_2^+ \rightarrow O_2^+ + CO \tag{48}$$

and

$$O^+ + CO_2 \rightarrow O_2^+ + CO. \tag{49}$$

As described by Fox (1985), Reaction (48) is more important below 150 km and Reaction (49) above 150 km. Reaction (49) has been studied in the laboratory (Walter et al. 1993) and has been shown to produce O_2^+ that is rotationally hot and vibrationally excited, with about 40% of the reaction exothermicity distributed statistically as internal excitation of the O_2^+ product. The resulting vibrational distribution is 38% in $v = 0$, 30% in $v = 1$, 18% in $v = 2$, and 15% in $v \geq 3$. Fox (1985) had earlier proposed that, above 150 km on Venus, dissociative recombination of excited vibrational levels of O_2^+ must be considered, because vibrational relaxation in collisions with CO_2 would be relatively slow. On Earth, O_2^+ is vibrationally relaxed by fast symmetric charge transfer collisions with O_2, which is improbable in the atmospheres of Mars and Venus.

Recently DR experiments have been performed at the CRYRING heavy-ion storage ring facility (Petrignani et al. 2005) using vibrationally defined molecular oxygen ions. The O_2^+ vibrational distribution was modified by varying the gas pressure, electron-beam voltage, and residence time in the ion source and measured by dissociative charge exchange in cesium vapor (Cosby et al. 2003; Petrignani et al. 2005). The results of these experiments are summarized in Table 5, from which we can see that both the DR cross section and the distribution of products are indeed strong functions of the vibrational quantum number.

Table 5 Partial relative cross sections, σ_v, quantum yields, and branching fractions for dissociative recombination of O_2^+ ($X^2\Pi_g$, $v = 0$–2), from Petrignani et al. (2005)

v	σ_v	Quantum yields			Blanching fractions			
		$O(^1S)$	$O(^1D)$	$O(^3P)$	$O(^1D) + O(^1S)$	$O(^1D) + O(^1D)$	$O(^3P) + O(^1D)$	$O(^3P) + O(^3P)$
0	1	0.06	0.94	1.00	5.8 ± 0.5	20.4 ± 0.3	47.3 ± 0.8	26.5 ± 0.8
1	0.31 ± 0.13	0.14	1.44	0.42	13.9 ± 3.1	51.0 ± 5.4	27.8 ± 5.1	7.3 ± 7.5
2	0.52 ± 0.16	0.21	1.02	0.76	21.1 ± 2.5	2.5 ± 2.1	76.4 ± 2.2	0.02 ± 0.03

3.6.2 Electron Impact Dissociative Excitation of O_2 and the Oxygen Airglow on Europa and Ganymede

Europa and Ganymede were observed to have an unsuspected ultraviolet dayglow dominated by the oxygen atomic emissions near 130.4 and 135.6 nm (Hall et al. 1995, 1998; Feldman et al. 2001). These observations confirmed the existence of a tenuous atmosphere (Broadfoot et al. 1979; Kumar and Hunten 1982; Hunten 1995), far less dense than thought earlier (Carlson et al. 1973; Yung and McElroy 1977). Using these emissions to infer information about the neutral atmosphere required quantitative information on relative yields of $O(2p^3 3s\ ^3P)$ and $O(2p^3 3s\ ^5P)$ from plausible oxygen sources, such as H_2O, O_2, and $O(^3P)$, excited by photons, electrons, or heavy particles. Water is an unlikely choice because its vapor pressure is extremely low at the relevant temperature. Hall et al. (1995) used the then available information on the collisions

$$e + O \rightarrow e + O^* \tag{50}$$

and

$$e + O_2 \rightarrow e + O + O^* \tag{51}$$

to calculate an expected ratio of emission strengths. Collision (51) gave an emission ratio $I(135.6)/I(130.4) = 1.9$, within the estimated uncertainty in the observed ratio, while Collision (50) gave an emission ratio 0.1.

These observations stimulated renewed interest in modeling these atmospheres and the surface impact processes that could produce a molecular oxygen atmosphere (Shematovich and Johnson 2001; Shematovich et al. 2005; Marconi 2007). Yung and McElroy (1977) had correctly indicated that any stream of energetic particles (photons, electrons, protons, etc., from the solar spectrum, solar wind, or jovian radiation environment) incident on an ice surface will eventually produce some H_2, which will quickly evaporate. The surface left behind will then have an oxygen excess, which will gradually produce some O_2, which will also evaporate. The UV dayglow observations also motivated new laboratory measurements (Noren et al. 2001a, 2001b; Kanik et al. 2003) and first-principles calculations (Zatsarinny and Tayal 2002).

3.7 Energetic Atomic/Molecular Collisions

As suggested in Sects. 2.4 and 2.5 above in this chapter, collisions of energetic heavy particles, from the solar wind or the local magnetized planetary environment, can deposit energy that may be observable as optical emissions, produce ionospheric modifications, or facilitate planetary escape. One good planetary science example is generation of X-ray emission from

comets resulting from charge exchange electron capture by multicharged ions in the solar wind (Otranto and Olson 2008). Here we critically review the available information on the specific case of ion-atom charge exchange collisions of hydrogen and oxygen atoms. See also the review by Lindsay and Stebbings (2005).

3.7.1 Degenerate Charge Exchange Collisions of H^+ *and* O^+ *with* H *and* O

Hydrogen and oxygen are among the most abundant elements in the universe. Correspondingly, their neutral atomic and ionized forms are primary components of interstellar clouds, the solar wind, and planetary magnetospheres and ionospheres. The fact that the ionization energies of H and O are nearly identical implies that the charge exchange collisions

$$H^+ + H \leftrightarrow H + H^+ \tag{52}$$

$$O^+ + O \leftrightarrow O + O^+ \tag{53}$$

$$O^+ + H \leftrightarrow O + H^+ \tag{54}$$

all have large reaction cross sections on the order of 10^{-15} cm^2 or greater from meV to keV collision energies.

H^+ from the solar wind, or precipitating from planetary magnetospheres, collides with H and O atoms in the upper atmospheres of Venus, Earth, and Mars. On Venus and Mars this is the origin of about 10% of exospheric ionization (Zhang et al. 1993). The sudden buildup of the magnetic field in the Martian bowshock is attributed to these charge exchange collisions in the Martian exosphere (Chen et al. 2001). Other effects of Reactions (52), (53), and (54) include the production of hot H and O atoms; facilitating the upward flow of H, H^+, O, and O^+, as well as interhemispheric transport of hydrogen; transferring kinetic energy to O and O^+; mediating magnetosphere-ionosphere energetic coupling; modifying the $[O^+]/[O]$ and $[H^+]/[H]$ ratios versus altitude; and limiting the lifetimes of O^+ and H^+ ions in the ring current colliding with hydrogen atoms in the geocorona.

The current knowledge of the cross section for collision (52) is summarized in Fig. 10, following the analysis of Huestis (2008). From the numerous laboratory experimental studies in the literature we have selected data for subsequent analysis from only two of the most recent (but still very old: McClure 1966; Wittkower et al. 1966) as the only that appear to be quantitatively reliable because on experiment-to-experiment consistency and agreement with theory. They cover the range from 2 to 250 keV. We lack high quality laboratory data at lower energies. From the various theoretical investigations at low collision energy we have also selected only a subset (Brinkman and Kramers 1930; Dalgarno and Yadav 1953; Jackson and Schiff 1953; Bates and Boyd 1962; Smith 1967; Hunter and Kuriyan 1977; Shakeshaft 1978; Olson 1983; Hodges and Breig 1991) for analysis. In this case, we have excluded some of the most reliable recent information (Davis and Thorson 1978; Krstic and Schultz 1999; Krstic et al. 2004; Furlanetto and Furlanetto 2007) because it presents more fine detail than our analysis can reproduce, and because it agrees quantitatively with the best low-energy data included, when degraded to the same energy resolution. Also shown in Fig. 10 is a piece-wise polynomial representation versus collision energy (Huestis 2008) that can be used for modeling studies. The formula is given in Table 6.

For Reaction (53) at low energies, three quantum theory investigations (Stallcop et al. 1991; Pesnell et al. 1993; Hickman et al. 1997a, 1997b) attempted to resolve disagreements between calculated collision frequencies at thermal energies with those inferred from ionospheric observations. The latter investigation, which included spin–orbit interactions,

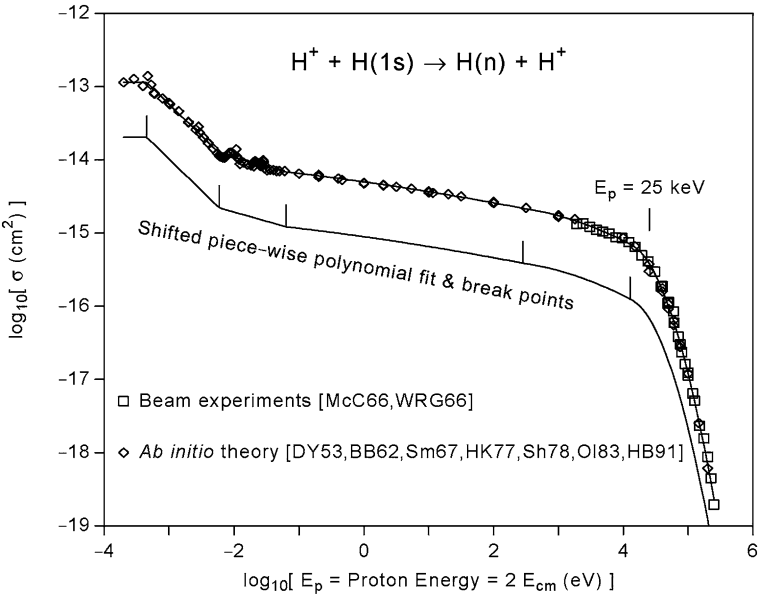

Fig. 10 Fitting the $H^+ + H$ Charge Transfer Cross Section, from Huestis (2008). The formula for the piece-wise polynomial fit is given in Table 6.
DY53 = Dalgarno and Yadav 1953; BB62 = Bates and Boyd 1962; McC66 = McClure 1966; WRG66 = Wittkower et al. 1966; Sm67 = Smith 1967; HK77 = Hunter and Kuriyan 1977; Sh78 = Shakeshaft 1978; Ol83 = Olson 1983; HB91 = Hodges and Breig 1991

gave results that were consistent with the earlier work for energies above 0.03 eV. At lower energies, spin–orbit interactions had a significant effect and the charge exchange and momentum transfer cross sections were no longer proportional.

For Reaction (54) at low energies, three quantum theory investigations (Chambaud et al. 1980; Stancil et al. 1999; Spirko et al. 2003) all included spin–orbit interactions. At energies above 0.03 eV, they agree with each other and calculations ignoring spin–orbit interactions agree with appropriate averages of spin–orbit-resolved cross sections. Below this energy, there are substantial differences, that are presumably due to different representations of the low-lying potential curves, spin–orbit couplings, charge-transfer matrix elements of the OH^+ molecule. Stancil et al. (1999) have provided explicit mathematical expressions that adequately represent the rate coefficients and cross sections for Reactions (54) from 0.1 to 10^6 eV.

4 Summary, Conclusions, and Recommendations

In this chapter we have followed the spirit expressed in the classic texts by Banks and Kockarts (1973), who supply the definitions

- Aeronomy is the scientific discipline devoted to the study of the composition, movement, and thermal balance of planetary atmospheres.
- As a field of research, aeronomy demands understanding of the basic concepts of both chemistry and physics as applied to a highly rarefied medium composed of neutral and charged particles.

Table 6 FORTRAN code fragment that returns values of the piece-wise linear fit for the cross section shown in Fig. 10 for the process $H^+ + H(1s) \rightarrow H(n\ell) + H^+$. Given the proton initial energy, `Ep`, in units of eV, `sigma( Ep )` returns the charge transfer cross section in units of cm^2

```
real function sigma( Ep )
x = alog10( Ep )
if( x .le. -3.3396 ) then
  y = -12.9451
else if( x .le. -2.2227 ) then
  y = -15.8262 -0.86272 * x
else if( x .le. -1.202 ) then
  y = -14.4664 -0.25094 * x
else if( x .le. 2.4513 ) then
  y = -14.3008 + ( -0.12455 -0.0094356 * x ) * x
else if( x .le. 4.1059 ) then
  y = -14.9562 + ( +0.36821 -0.10138 * x ) * x
else
  y = -43.9887 + ( +14.4120 -1.79965 * x ) * x
end if
sigma = 10.0**y
return
end
```

Here we have followed their emphasis on what we know, or wish we knew, about the fundamental underlining microscopic chemical and collisional processes, based on, or confirmed by, laboratory measurements and first-principles theory calculations, that are documented in the published peer-reviewed literature. Correspondingly we make the following recommendations,

- Laboratory experiments and first-principles theory calculations are essential components of planetary aeronomy research programs, comparable in importance to observational and modeling efforts.
- Critical evaluation and documentation of the current state of knowledge or ignorance of the microscopic chemical and collisional processes are of comparable importance to "original research" because they provide essential guidance and constraints on interpretative and modeling attempts to "explain" surprising or unexpected observations.

References

W.A. Abdou, D.G. Torr, P.G. Richards, M.R. Torr, E.L. Breig, J. Geophys. Res. **89**(A10), 9069–9079 (1984)
R.A. Akmaev, J. Geophys. Res. **108**(A7), 1292 (2003). doi:10.1029/2003JA009896
M.J. Alexander, A.I.F. Stewart, S.C. Solomon, S.W. Bougher, J. Geophys. Res. **98**(E6), 10,849–10,871 (1993)
V.G. Anicich, An index of the literature for bimolecular gas phase cation-molecule. Reaction kinetics. JPL Publication 03-19 (2003). trs-new.jpl.nasa.gov/dspace/bitstream/2014/7981/1/03-2964.pdf
V.G. Anicich, M.J. McEwan, Planet. Space Sci. **45**, 897–921 (1997)
S.K. Atreya, T.M. Donahue, J.H. Waite Jr., Nature **280**, 795–796 (1979)
G.E. Ballester, M.A. McGrath, D.F. Strobel, X. Zhu, P.D. Feldman, H.W. Moos, Icarus **111**, 2–17 (1994)
P.M. Banks, G. Kockarts, *Aeronomy, Parts A and B* (Academic Press, New York, 1973)
C.A. Barth, JPL Res. Summ. 36–39 **1**, 64 (1961)

C.A. Barth, The photochemistry of the atmosphere of Mars, in *The Photochemistry of Atmospheres*, ed. by J.S. Levine (Academic Press, New York, 1985)
C.A. Barth, C.W. Hord, J.B. Pearce, K.K. Kelly, G.P. Anderson, A.I. Stewart, J. Geophys. Res. **76**(10), 2213–2227 (1971)
J.N. Bass, J. Chem. Phys. **60**, 2913–2921 (1974)
D.R. Bates, Planet. Space Sci. **38**, 889–902 (1990)
D.R. Bates, A.H. Boyd, Proc. Phys. Soc. **80**, 1301–1307 (1962)
S.J. Bauer, *Physics of Planetary Ionospheres* (Springer, Berlin, 1973)
D.L. Baulch, D.D. Drysdale, J. Duxbury, S.J. Grant, *Evaluated Kinetic Data for High Temperature Reactions*, vol. 3 (Butterworths, London, 1976)
N.H.F. Beebe, E.W. Thulstrup, A. Andersen, J. Chem. Phys. **64**, 2080–2093 (1976). Supplementary Data Tables (private communication)
Y. Bénilan, N. Smith, A. Jolly, F. Raulin, Planet. Space Sci. **48**, 463–471 (2000)
J. Berkowitz, *Atomic and Molecular Photoabsorption – Absolute Total Cross Sections* (Academic Press, New York, 2002)
J.-L. Bertaux, F. Leblanc, S. Perrier, E. Quemerais, O. Korablev, E. Dimarellis, A. Reberac, F. Forget, P.C. Simon, S.A. Stern, B. Sandel, the SPICAM team, Science **307**, 566–569 (2005)
H.A. Bethe, Rev. Mod. Phys. **9**, 69–249 (1937)
B. Bezard, H. Feuchtgruber, J.I. Moses, T. Encrenaz, Astron. Astrophys. **334**, L41–L44 (1998)
B. Bezard, P.N. Romani, H. Feuchtgruber, T. Encrenaz, Astrophys. J. **515**, 868–872 (1999)
N.K. Bibinov, F.I. Vilesov, I.P. Vinogradov, L.D. Mineev, A.M. Pravilov, Sov. J. Quantum Electron. **9**, 838–844 (1979)
A.P. Billingham, P. Borrell, J. Chem. Soc. Faraday Trans. 2 **82**, 963–970 (1986)
D. Blackie, R. Blackwell-Whitehead, G. Stark, J.C. Pickering, J. Rufus, A. Thorne, P. Smith, Sulphur dioxide: high resolution ultra-violet photoabsorption cross section measurements at 200 K. Eos Trans. AGU **88**(52). Fall Meet. Suppl., Abstract P21A-0226 (2007)
P. Borrell, P.M. Borrell, M.D. Pedley, K.R. Grant, Proc. R. Soc. Lond. **367**, 395–410 (1979)
P.M. Borrell, P. Borrell, K.R. Grant, M.D. Pedley, J. Phys. Chem. **86**, 700–703 (1982)
S.W. Bougher, W.J. Borucki, J. Geophys. Res. **99**(E2), 3759–3776 (1994)
S.W. Bougher, J.C. Gerard, A.I.F. Stewart, C.G. Fesen, J. Geophys. Res. **95**(A5), 6271–6284 (1990)
S.W. Bougher, M.J. Alexander, H.G. Mayr, Upper atmosphere dynamics: Global circulation and gravity waves, in *Venus II*, ed. by S.W. Bougher, D.M. Hunten, P.J. Phillips (U. Arizona Press, Tucson, 1997), pp. 259–292
S.W. Bougher, S. Engel, R.G. Roble, B. Foster, J. Geophys. Res. **104**(E7), 16,591–16,611 (1999)
S.W. Bougher, S. Engel, R.G. Roble, B. Foster, J. Geophys. Res. **105**(E7), 17669–17692 (2000)
S.W. Bougher, R.G. Roble, T.J. Fuller-Rowell, Simulations of the upper atmospheres of the terrestrial planets, in *Atmospheres in the Solar System – Comparative Aeronomy*, M. Mendillo, A. Nagy, J.H. Waite, eds., AGU Monograph **130**, 261–288 (2002)
S.W. Bougher, S. Rafkin, P. Drossart, Planet. Space Sci. **54**, 1371–1380 (2006a)
S.W. Bougher, J.M. Bell, J.R. Murphy, M.A. Lopez-Valverde, P.G. Withers, Geophys. Res. Lett. **33**, L02203 (2006b)
M.T. Bowers, W.H. Chesnavich, W.T. Huntress Jr., Int. J. Mass Spectrom. Ion Phys. **12**, 357–382 (1973)
H.C. Brinkman, H.A. Kramers, Proc. Acad. Sci. Amst. **33**, 973–984 (1930)
A.L. Broadfoot et al., Science **204**, 979–982 (1979)
R.A. Brownsword, M. Hillenkamp, T. Laurent, R.K. Vasta, H.-R. Volpp, J. Wolfrum, Chem. Phys. Lett. **266**, 259–266 (1997)
I.M. Campbell, C.N. Gray, Chem. Phys. Lett. **18**, 607–609 (1973)
I.M. Campbell, B.A. Thrush, Proc. R. Soc. A **296**, 222–232 (1967)
M.T. Capria, G. Cremonese, A. Bhardwaj, M.C. de Sanctis, Astron. Astrophys. **442**, 1121–1126 (2005)
M.T. Capria, G. Cremonese, A. Bhardwaj, M.C. de Sanctis, E. Mazzotta Epifani, Astron. Astrophys. **479**, 257–263 (2008)
R.W. Carlson et al., Science **182**, 53–55 (1973)
K.J. Castle, K.M. Kleissas, J.M. Rhinehart, E.S. Hwang, J.A. Dodd, J. Geophys. Res. **111**, A09303 (2006)
G. Chambaud, J.M. Launay, B. Lefy, P. Millie, E. Roueff, F. Tran Minh, J. Phys. B **13**, 4255–4216 (1980)
W.F. Chan, G. Cooper, C.E. Brion, Chem. Phys. **178**, 387–400 (1993)
T. Chang, D.G. Torr, P.G. Richards, S.C. Solomon, J. Geophys. Res. **98**(A9), 15,589–15,597 (1993)
M. Chatelet, A. Tardieu, W. Spreitzer, M. Maier, Chem. Phys. **102**, 387–394 (1986)
F.Z. Chen, C.Y.R. Wu, J. Quant. Spectrosc. Radiat. Transfer **85**, 195–209 (2004)
F.Z. Chen, D.L. Judge, C.Y.R. Wu, J. Caldwell, H.P. White, R. Wagener, J. Geophys. Res. **96**, 17519–17527 (1991)
F.Z. Chen, D.L. Judge, C.Y.R. Wu, Chem. Phys. **260**, 215–223 (2000)

Y. Chen, P.A. Cloutier, D.H. Crider, C. Mazelle, H. Reme, J. Geophys. Res. **106**(A12), 29,387–29,399 (2001)
A.L. Cochran, W.D. Cochran, Icarus **154**, 381–390 (2001)
J.E.P. Connerney, J.H. Waite, Nature **312**, 136–138 (1984)
P.A. Cook, M.N.R. Ashfold, Y.J. Jee, K.H. Jung, S. Harich, X.M. Yang, Phys. Chem. Chem. Phys. **3**, 1848–1860 (2001)
M. Cordonnier, D. Uy, R.M. Dickson, K.E. Kerr, Y. Zhang, T. Oka, J. Chem. Phys. **113**, 3181–3193 (2000)
P.C. Cosby, J.R. Peterson, D.L. Huestis, Dissociative recombination of vibrationally excited levels in oxygen molecular ions, in *Dissociative Recombination of Molecular Ions with Electrons*, ed. by S.L. Guberman (Kluwer/Plenum, New York, 2003), pp. 101–108
C. Cossart-Magos, S. Leach, M. Eidelsberg, F. Launay, R. Rostas, J. Chem. Soc. Faraday Trans. **78**(2), 1477–1487 (1982)
C. Cossart-Magos, M. Jungen, F. Launay, Molec. Phys. **61**, 1077–1117 (1987)
T.E. Cravens, Astrophysical applications for electron energy deposition in molecular hydrogen. Ph.D. thesis, Harvard University, Cambridge, MA (1974)
T.E. Cravens, J. Geophys. Res. **92**(A10), 11,083–11,100 (1987)
T.E. Cravens et al., Geophys. Res. Lett. **33**, L07105 (2006)
A. Dalgarno, H.N. Yadav, Proc. Phys. Soc. **A66**, 173–177 (1953)
E.I. Dashevskaya, E.E. Nikitin, Chem. Phys. Lett. **328**, 119–123 (2000)
E.I. Dashevskaya, J.A. Kunc, E.E. Nikitin, I. Oref, J. Chem. Phys. **118**, 3141–3147 (2003)
E.I. Dashevskaya, I. Litvin, E.E. Nikitin, J. Troe, J. Chem. Phys. **125**, 154315 (2006)
E.I. Dashevskaya, I. Litvin, E.E. Nikitin, J. Troe, J. Chem. Phys. **127**, 114317 (2007)
J.P. Davis, W.R. Thorson, Can. J. Phys. **56**, 996–1020 (1978)
S.P. Davis, M.C. Abrams, J.W. Brault, *Fourier Transform Spectrometry* (Academic Press, New York, 2001)
A.H. Delsemme, Photodissociation of CO_2 into CO + O(^{1}D), in *Les Spectres des Molécules Simples au Laboratorie et en Astrophysique* (Liège Institut d'Astrophysique, Université de Liège, Liège, 1980), pp. 515–523
G.S. Diskin, Experimental and theoretical investigation of the physical processes important to the RELIEF flow tagging diagnostic. Ph.D. Thesis, Princeton University (1997)
G.S. Diskin, W.R. Lempert, R.B. Miles, Observation of vibrational dynamics in $X3\Sigma_g^-$ oxygen following stimulated Raman excitation to the $v = 1$ Level: Implications for the RELIEF Flow Tagging Technique. AIAA 96-3001, 34th Aerospace Sciences Meeting and Exhibit (Reno, NV, 15–18 January 1996)
J.A. Dodd, E.S. Hwang, M. Simione, K.J. Castle, Laboratory measurement of $CO_2(v_2)$ + O temperature-dependent vibrational energy transfer. Eos Trans. AGU **88**(52), Fall Meet. Suppl., Abstract SA41A-0278 (2007); private communication; K.J. Castle, L.A. Black, M.W. Simione, E.S. Hwang, J.A. Dodd (manuscript in preparation)
P. Drossart et al., Nature **340**, 539–542 (1989)
V. Escalante, G.A. Victor, Planet. Space Sci. **40**, 1705–1718 (1992)
A. Fahr, A.K. Nayak, Chem. Phys. **189**, 725–731 (1994)
A. Fahr, A. Nayak, Chem. Phys. **203**, 351–358 (1996)
B. Faltermeier, R. Protz, M. Maier, Chem. Phys. **62**, 377–385 (1981)
P.D. Feldman, M.A. McGrath, D.F. Strobel, H.W. Moos, K.D. Retherford, B.C. Wolven, Astrophys. J. **535**, 1085–1090 (2001)
M.C. Festou, Astron. Astrophys. **96**, 52–57 (1981)
M.C. Festou, P.D. Feldman, Astron. Astrophys. **103**, 154–159 (1981)
J.-H. Fillion, J. Ruiz, X.-F. Yang, M. Castillejo, F. Rostas, J.-L. Lemaire, J. Chem. Phys. **120**, 6531–6541 (2004)
J.L. Fox, Adv. Space Res. **5**(9), 165–169 (1985)
J.L. Fox, Planet. Space Sci. **36**, 37–46 (1988)
J.L. Fox, Chemistry of the atmosphere: ion chemistry, in *Encyclopedia of Atmospheric Sciences*, ed. by J.R. Holton, J. Pyle, J.A. Curry (Elsevier, London, 2002), pp. 359–375
J.L. Fox, Aeronomy, in *Springer Handbook of Atomic, Molecular, and Optical Physics*, ed. by G.W.F. Drake (Springer, New York, 2006), pp. 1259–1292, Chapter 84
J.L. Fox, A. Dalgarno, J. Geophys. Res. **84**(A12), 7315–7331 (1979)
J.L. Fox, A. Dalgarno, J. Geophys. Res. **88**, 9027–9032 (1983)
J.L. Fox, R.V. Yelle, Geophys. Res. Lett. **24**, 2179–2182 (1997)
J.L. Fox, P. Zhou, S.W. Bougher, Adv. Space Res. **17**, (11)203–(11)218 (1995)
J.L. Fox et al., Energy deposition, Space Sci. Rev. (2008, this issue). Chapter 1
A.H. Friedson, A.-S. Wong, Y.L. Yung, Icarus **158**, 389–400 (2002)
S.R. Furlanetto, M.R. Furlanetto, Mon. Not. R. Astron. Soc. **374**, 547–555 (2007)
M. Galand, S. Chakrabarti, Auroral processes in the solar system, in *Atmospheres in the Solar System – Comparative Aeronomy*, ed. by M. Mendillo, A. Nagy, J.H. Waite, AGU Monograph **130**, 55–76 (2002)

M. Galand, S. Chakrabarti, J. Atmos. Solar Terr. Phys. **68**, 1488–1501 (2006)
M. Galand, D. Lummerzheim, J. Geophys. Res. **109**, A03307 (2004)
T.R. Geballe, M.F. Jagod, T. Oka, Astrophys. J. **408**, L109–L112 (1993)
J. Gerard, A. Saglam, G. Piccioni, P. Drossart, C. Cox, S. Erard, R. Hueso, A. Sanchez-Lavega, The distribution of the O_2 infrared nightglow observed with VIRTIS on board Venus Express. Geophys Res. Lett. (2008, in press). doi:10.1029/2007GL032021
D. Gerlich, E. Herbst, E. Roueff, Planet. Space Sci. **50**, 1275–1285 (2002)
G.A. Germany, D. Lummerzheim, P.G. Richards, J. Geophys. Res. **106**, 12,837–12,843 (2001)
K. Giles, N.G. Adams, D. Smith, J. Phys. Chem. **96**, 7645–7650 (1992)
G.R. Gladstone, J. Geophys. Res. **97**, 1377–1387 (1992)
G.R. Gladstone, M. Allen, Y.L. Yung, Icarus **119**, 1–52 (1996)
J. Glosik, A.B. Rakshit, N.C. Twiddy, N.G. Adams, D. Smith, J. Phys. B **11**, 3365–3379 (1978)
D. Grodent, J.H. Waite Jr., J.-C. Gerard, J. Geophys. Res. **106**(A7), 12,933–12,952 (2001)
D.T. Hall, D.F. Strobel, P.D. Feldman, M.A. McGrath, H.A. Weaver, Nature **373**, 677–679 (1995)
D.T. Hall, P.D. Feldman, M.A. McGrath, D.F. Strobel, Astrophys. J. **499**, 475–481 (1998)
J.T. Hallett, D.E. Shemansky, X. Liu, The Cassini UVIS Team, Cassini UVIS observations of the Saturn H_2 dayglow emission. Eos Trans. AGU **85**(47), F1268 (2004)
J.T. Hallett, D.E. Shemansky, X. Liu, Geophys. Res. Lett. **32**, L02204 (2005a)
J.T. Hallett, D.E. Shemansky, X. Liu, Astrophys. J. **624**, 448–461 (2005b)
W.B. Hanson, S. Sanatani, D.R. Zuccaro, J. Geophys. Res. **82**, 4351–4363 (1977)
N.M. Harvey, Chem. Phys. Lett. **88**, 553–558 (1982)
A.J.R. Heck, R.N. Zare, D.W. Chandler, J. Chem. Phys. **104**, 4019–4030 (1996)
A.E. Hedin, H.B. Niemann, W.T. Kasprzak, A. Seiff, J. Geophys. Res. **88**, 73–83 (1983)
A.P. Hickman, M. Medikeri-Naphade, C.D. Chapin, D.L. Huestis, Geophys. Res. Lett. **24**, 119–122 (1997a)
A.P. Hickman, M. Medikeri-Naphade, C.D. Chapin, D.L. Huestis, Phys. Rev. A **56**, 4633–4643 (1997b)
R.R. Hodges Jr., E.L. Breig, J. Geophys. Res. **96**(A5), 7697–7708 (1991)
R.D. Hudson, Rev. Geophys. Space Phys. **9**, 305–406 (1971)
W.F. Huebner, "The photochemistry of comets" and Appendix "Unattenuated solar photo rate coefficients at 1 AU heliocentric distance", in *The Photochemistry of Atmospheres*, ed. by J.S. Levine (Academic Press, New York, 1985)
D.L. Huestis, Current laboratory experiments for planetary aeronomy, in *Atmospheres in the Solar System – Comparative Aeronomy*, M. Mendillo, A. Nagy, J.H. Waite, eds., AGU Monograph **130**, 245–258 (2002)
D.L. Huestis, Chem. Phys. Lett. **411**, 108–110 (2005a)
D.L. Huestis, $H^+ + H_2$ ion-molecule reactions in the ionospheres of the outer planets. Bull. Am. Astron. Soc. **37**, 757 (2005b)
D.L. Huestis, J. Phys. Chem. **110**, 6638–6642 (2006a)
D.L. Huestis, Radiative transition probabilities, in *Springer Handbook of Atomic, Molecular, and Optical Physics*, ed. by G.W.F. Drake (Springer, New York, 2006b), pp. 515–533, Chapter 33
D.L. Huestis, Hydrogen collisions in planetary atmospheres, ionospheres, and magnetospheres. AOGS 2007 Proceedings, Planet. Space Sci. (2008, in press)
D.L. Huestis, J. Berkowitz, Photoabsorption cross sections for polyatomic molecules in planetary atmospheres. SRI International proposal PYU 07-091 submitted to NASA Planetary Atmospheres (June 2007)
D.L. Huestis, J.M. Bowman, Vibrationally excited H_3^+ in outer planet atmospheres. SRI International proposal PYU 07-173 submitted to NASA Outer Planets Research (November 2007)
D.L. Huestis, T.G. Slanger, Cross sections and yields of $O(^1S)$ and $O(^1D)$ in photodissociation of H_2O and CO_2. Bull. Am. Astron. Soc. **38**, 609 (2006)
D.L. Huestis, G. Black, S.A. Edelstein, R.L. Sharpless, J. Chem. Phys. **60**, 4471–4474 (1974)
D.L. Huestis, J. Marschall, G.D. Billing, R. Maclagan, Theoretical and experimental studies of O–CO_2 collisions. Eos Trans. AGU **83**, F1106 (2002)
D.L. Huestis, B.D. Sharpee, T.G. Slanger, Eos Trans. AGU **88**(52) (2007). Fall Meet. Suppl., Abstract SA41-0261
D.M. Hunten, Planet. Space Sci. **30**, 773–783 (1982)
D.M. Hunten, Nature **373**, 654 (1995)
G. Hunter, M. Kuriyan, Proc. R. Soc. Lond. A **353**, 575–588 (1977)
W.T. Huntress Jr., V.G. Anicich, Astrophys. J. **208**, 237–244 (1976)
A. Ichihara, O. Iwamoto, R.K. Janev, J. Phys. B **33**, 4747–4758 (2000)
J.D. Jackson, H. Schiff, Phys. Rev. **89**, 359–365 (1953)
R.K. Janev, D. Reiter, U. Samm, Collision processes in low-temperature hydrogen plasmas (2003). http://www.eirene.de/reports/report_4105.pdf

K.L. Jessup, J. Spencer, R. Yelle, Icarus **192**, 24–40 (2007)
R. Johnsen, M.A. Biondi, Geophys. Res. Lett. **7**, 401–403 (1980a)
R. Johnsen, M.A. Biondi, J. Chem. Phys. **73**, 190–193 (1980b)
R.E. Johnson, *Energetic Charged Particle Interactions with Atmospheres and Surfaces* (Springer, Berlin, 1990)
R.E. Johnson, M. Liu, C. Tully, Planet. Space Sci. **50**, 123–128 (2002)
P.V. Johnson, C.P. Malone, I. Kanik, K. Tran, M.A. Khakoo, J. Geophys. Res. **110**, A11311 (2005)
R.E. Johnson et al., Exospheres. Space Sci. Rev. (2008, this issue). Chapter 9
D.B. Jones, L. Campbell, M.J. Bottema, P.J.O. Teubner, D.C. Cartwright, W.R. Newell, M.J. Brunger, Planet. Space Sci. **54**, 45–59 (2006)
I. Kanik, C. Noren, O.P. Vattipalle, J.M. Ajello, D.E. Shemansky, J. Geophys. Res. **108**(E11), 5126 (2003)
G.P. Karwasz, T. Wroblewski, R.S. Brusa, E. Illenberger, Jpn. J. Appl. Phys. **45**, 8192–8196 (2006)
D. Kella, L. Vejby-Christensen, P.J. Johnson, H.B. Pederson, L.H. Andersen, Science **276**, 1530–1533 (1997)
C.N. Keller, V.G. Anicich, T.E. Cravens, Planet. Space Sci. **46**, 1157–1174 (1998)
H. Keller-Rudek, G.K. Moortgat, MPI-Mainz-UV-VIS Spectral Atlas of Gaseous Molecules (2008). http://www.atmosphere.mpg.de/enid/2295
V. Kharchenko, A. Dalgarno, B. Zygelman, J.-H. Yee, J. Geophys. Res. **103**, 24,899–24,906 (2000)
V. Kharchenko, A. Dalgarno, D.R. Schultz, P.C. Stancil, Geophys. Res. Lett. **33**, L11105 (2006)
L.E. Khvorostovskaya, I.Yu. Potekhin, G.M. Shved, V.P. Ogibalov, T.V. Uzyukova, Izvestiya Atmos. Ocean. Phys. **38**, 613–624 (2002)
Y.H. Kim, J.L. Fox, Icarus **112**, 310–325 (1994)
J.K. Kim, L.P. Heard, W.T. Huntress Jr., Int. J. Mass Spectr. Ion Phys. **15**, 223–244 (1974)
Y.H. Kim, J.L. Fox, H.S. Porter, J. Geophys. Res. **97**(E4), 6093–6101 (1992)
H. Klingshirn, B. Faltermeier, W. Hengl, M. Maier, Chem. Phys. Lett. **93**, 485–489 (1982)
H. Klingshirn, M. Maier, J. Chem. Phys. **82**, 714–719 (1985)
M.B. Knickelbein, K.L. Marsh, O.E. Ulrich, G.E. Busch, J. Chem. Phys. **87**, 2392–2393 (1987)
V.D. Knyazev, I.R. Slagle, J. Phys. Chem. **100**, 16899–16911 (1996)
I. Koyano, T.S. Wauchop, K.H. Welge, J. Chem. Phys. **63**, 110–112 (1973)
V.A. Krasnopolsky, D.P. Cruikshank, J. Geophys. Res. **100**(E10), 21,271–21,286 (1995)
P.S. Krstic, Phys. Rev. A **66**, 042717 (2002)
P.S. Krstic, D.R. Schultz, J. Phys. B **32**, 3485–3509 (1999)
P.S. Krstic, D.R. Schultz, J. Phys. B **36**, 385–398 (2003)
P.S. Krstic, D.R. Schultz, R.K. Janev, Phys. Scripta **T96**, 61–71 (2002)
P.S. Krstic, J.H. Macek, S.Yu. Ovchinnikov, D.R. Schulz, Phys. Rev. A **70**, 042711 (2004)
S. Kumar, D.M. Hunten, The atmospheres of Io and other satellites, in *Satellites of Jupiter*, ed. by D. Morrison (U. Arizona Press, Tucson, 1982)
L. Landau, E. Teller, Zur Theorie der Schalldispersion. Phys. Z. Sowjet. **10**, 34–43 (1936) [trans. D. Ter Haar, *Collected Papers of L.D. Landau* (Gordon and Breach, New York, 1965)]
M.P. de Lara-Castells, M.I. Hedrnandez, G. Delgado-Barrio, P. Villarreal, M. Lopez-Puertas, J. Chem. Phys. **124**, 164302 (2006)
M.P. de Lara-Castells, M.I. Hedrnandez, G. Delgado-Barrio, P. Villarreal, M. Lopez-Puertas, Molec. Phys. **105**, 1171–1181 (2007)
G.M. Lawrence, J. Chem. Phys. **57**, 5616–5617 (1972)
R.C.M. Learner, A.P. Thorne, J. Opt. Soc. Am. B **5**(10), 2045–2059 (1988)
S.A. Ledvina et al., Modelling of plasma flows and related phenomena. Space Sci. Rev. (2008, this issue). Chapter 4
A.Y.T. Lee, Y.L. Yung, J. Moses, J. Geophys. Res. **105**(E8), 20,207–20,225 (2000)
E. Lellouch, Phil. Trans. R. Soc. Lond. A **364**, 3139–3146 (2006)
E. Lellouch, T. Clancy, D. Crisp, A. Kliore, D. Titov, S.W. Bougher, Monitoring of mesospheric structure and dynamics, in *Venus II*, ed. by S.W. Bougher, D.M. Hunten, P.J. Phillips (U. Arizona Press, Tucson, 1997), pp. 295–324
B.R. Lewis, J.H. Carver, J. Quant. Spectrosc. Radiat. Transfer **30**, 297–309 (1983)
X. Li, Y.-L. Huang, G.D. Flesch, C.Y. Ng, J. Chem. Phys. **104**, 1373–1381 (1997)
H.V. Lilenfeld, Deactivation of vibrationally excited NO and CO_2 by O-atoms. Final report PL-TR-94-2180 (McDonnell Douglas Corp., St. Louis, June 1994)
B.G. Lindsay, R.F. Stebbings, J. Geophys. Res. **110**, A12213 (2005)
X. Liu, D.E. Shemansky, J. Geophys. Res. **111**, A04303 (2006)
D. Lummerzheim, M. Galand, J. Semeter, M.J. Mendillo, M.H. Rees, F.J. Rich, J. Geophys. Res. **106**, 141–148 (2001)
H. Luna, M. Michael, M.B. Shah, R.E. Johnson, C.J. Latimer, J.W. McConkey, J. Geophys. Res. **108**(E4) (2003). doi:10.1029/2002JE001950

H. Luna, C. McGrath, M.B. Shah, R.E. Johnson, M. Liu, C.J. Latimer, E.C. Montenegro, Astrophys. J. **628**, 1086–1096 (2005)
J.R. Lyons, Y.L. Yung, M. Allen, Science **256**, 204–206 (1992)
M.T. MacPherson, M.J. Pilling, M.J.C. Smith, Chem. Phys. Lett. **94**, 430–433 (1983)
M.T. MacPherson, M.J. Pilling, M.J.C. Smith, J. Phys. Chem. **89**, 2268–2274 (1985)
T. Majeed, J.C. McConnell, D.F. Strobel, M.E. Summers, Geophys. Res. Lett. **17**, 1721–1724 (1990)
T. Majeed, J.H. Waite Jr., S.W. Bougher, R.V. Yelle, G.R. Gladstone, J.C. McConnell, A. Bhardwaj, Adv. Space Res. **33**, 197–211 (2004)
M.L. Marconi, Icarus **190**, 155–174 (2007)
S.L. Manatt, A.L. Lane, J. Quant. Spectrosc. Radiat. Transf. **50**, 267–276 (1993)
A.N. Maurellis, T.E. Cravens, Icarus **154**, 350–371 (2001)
G.E. McClure, Phys. Rev. **148**, 47–54 (1966)
J.C. McConnell, T. Majeed, J. Geophys. Res. **92**(A8), 8570–8578 (1987)
J.C. McConnell, J.B. Holdberg, G.R. Smith, B.R. Sandel, D.E. Shemansky, A.L. Broadfoot, Planet. Space Sci. **30**, 151–167 (1982)
M.B. McElroy, Space Sci. Rev. **14**, 460–473 (1973)
M.B. McElroy, D.M. Hunten, J. Geophys. Res. **75**, 1188–1201 (1970)
M.A. McGrath, M.J.S. Belton, J.R. Spencer, P. Sartoretti, Icarus **146**, 476–493 (2000)
T.B. McMahon, P.G. Miasek, J.I. Beauchamp, Int. J. Mass Spectrom. Ion Phys. **21**, 63–71 (1976)
J.R. McNesby, I. Tanaka, H. Okabe, J. Chem. Phys. **36**, 605–607 (1962)
H. Melin, S. Miller, T. Stallard, D. Grodent, Icarus **178**, 97–103 (2005)
H. Melin, S. Miller, T. Stallard, C. Smith, D. Grodent, Icarus **181**, 256–265 (2006)
M. Michael, R.E. Johnson, Planet. Space Sci. **53**, 1510–1514 (2005)
R.L. Miller, S.H. Kable, P.L. Houston, I. Burak, J. Chem. Phys. **96**, 332–338 (1992)
S. Miller et al., Phil. Trans. R. Soc. Lond. A **358**, 2485–2512 (2000)
S. Miller, T. Stallard, C. Smith, G. Millward, H. Melin, M. Lystrup, A. Aylward, Phil. Trans. R. Soc. Lond. A **364**, 3121–3137 (2006)
J.B.A. Mitchell, S.L. Guberman (eds.), *Dissociative Recombination: Theory, Experiment, and Application* (World Scientific, NJ, 1989)
L.E. Moore, M. Mendillo, I.C.F. Müller-Wodarg, D.L. Murr, Icarus **172**, 503–520 (2004)
L. Moore, A.F. Nagy, A.J. Kliore, I. Müller-Wodarg, J.D. Richardson, M. Mendillo, Geophys. Res. Lett. **33**, L22202 (2006)
D.H. Mordaunt, I.R. Lambert, G.P. Morley, M.N.R. Ashford, R.N. Dixon, C.M. Western, J. Chem. Phys. **98**, 2054–2065 (1993)
J.E. Morgan, H.I. Schiff, J. Chem. Phys. **38**, 1495–1500 (1963)
J.E. Morgan, L. Elias, H.I. Schiff, J. Chem. Phys. **33**, 930–931 (1960)
J.I. Moses, S.F. Bass, J. Geophys. Res. **105**(E3), 7013–7052 (2000)
J.I. Moses, T. Fouchet, R.V. Yelle, A.J. Friedson, G.S. Orton, B. Bézard, P. Drossart, G.R. Gladstone, T. Kostiuk, T.A. Livengood, The stratosphere of Jupiter, in *Jupiter: Planet, Satellites and Magnetosphere*, ed. by F. Bagenal, T.E. Dowling, W.B. McKinnon (Cambridge Univ. Press, New York, 2004), pp. 129–157
J.I. Moses, T. Fouchet, B. Bézard, G.R. Gladstone, E. Lellouch, H. Feuchtgruber, J. Geophys. Res. **110**, E08001 (2005)
R. Mota, R. Parafita, A. Giuliani, M.-J. Hubin-Franskin, J.M.C. Lourenco, G. Garcia, S.V. Hoffman, N.J. Mason, P.A. Ribeiro, M. Paposo, P. Limao-Vieira, Chem. Phys. Lett. **416**, 152–159 (2005)
G.E. Moyano, M.A. Collins, J. Chem. Phys. **119**, 5510–5517 (2003)
J.E. Murray, High resolution spectrometry of neutral chromium using a Fourier transform spectrometer. Ph.D Thesis, Imperial College, London University (1992)
A.F. Nagy, T.E. Cravens, Solar system ionospheres, in *Atmospheres in the Solar System – Comparative Aeronomy*, ed. by M. Mendillo, A. Nagy, J.H. Waite, AGU Monograph **130**, 39–54 (2002)
H. Nair, M. Allen, A.D. Anbar, Y.L. Yung, R.T. Clancy, Icarus **111**, 124–150 (1994)
R.S. Nakata, K. Watanabe, F.M. Matsunaga, Sci. Light **14**(1), 54–71 (1965)
H.B. Niemann, R.E. Hartle, A.E. Hedin, W.T. Kasprzak, N.W. Spencer, D.M. Hunten, G.R. Carignan, Science **205**, 54–56 (1979)
H.B. Niemann, W.T. Kasprzak, A.E. Hedin, D.M. Hunten, N.W. Spencer, J. Geophys. Res. **85**, 7817–7827 (1980)
E.E. Nikitin, J. Troe, Phys. Chem. Chem. Phys. **125**, 154315 (2006)
E.E. Nikitin, S.Ya. Umanski, Faraday Disc. Chem. Soc. **53**, 7–17 (1972)
C. Noren, I. Kanik, J.M. Ajello, P. McCartney, O.P. Makarov, W.E. McClintock, V.A. Drake, Geophys. Res. Lett. **28**, 1379–1392 (2001a)
C. Noren, I. Kanik, P.V. Johnson, P. McCartney, G.K. James, J.M. Ajello, J. Phys. B **34**, 2667–2677 (2001b)

M. Ogawa, J. Chem. Phys. **54**, 2550–2556 (1971)
T. Oka, Phys. Rev. Lett. **45**, 531–534 (1980)
T. Oka, J. Molec. Spectrosc. **228**, 635–639 (2004)
T. Oka, E. Epp, Astrophys. J. **613**, 349–354 (2004)
T. Oka, T.R. Geballe, Astrophys. J. **351**, L53–L56 (1990)
H. Okabe, *Photochemistry of Small Molecules* (Wiley, New York, 1978)
R.E. Olson, Phys. Rev. A **27**, 1871–1878 (1983)
E.R. O'Neill, B.D. Sharpee, T.G. Slanger, The nightglow content of astronomical spectra taken during the October/November 2003 solar storm. Eos Trans. AGU **87**(52). Fall Meet. Suppl., Abstract SA13B-0277 (2006)
S. Otranto, R.E. Olson, Phys. Rev. A **77**, 022709 (2008)
M.K. Pandey, R.K. Dubey, D.N. Tripathi, Eur. Phys. J. D **45**, 273–277 (2007)
K. Park, J.C. Light, J. Chem. Phys. **126**, 044305 (2007)
D.A. Pejaković, K.S. Kalogerakis, R.A. Copeland, D.L. Huestis, R.M. Robertson, G.P. Smith, Rate coefficients for O-atom three-body recombination in N_2 at temperatures in the range 170–320 K. Eos Trans. AGU **86**(52) Fall Meet. Suppl. Abstract SA53B-1172 (2005)
D.A. Pejaković, K.S. Kalogerakis, R.A. Copeland, D.L. Huestis, J. Geophys. Res. **113**, A04303 (2008)
W.D. Pesnell, K. Omidvar, W.R. Hogey, Geophys. Res. Lett. **20**, 1343–1356 (1993)
A. Petrignani, W.J. van der Zande, P.C. Cosby, F. Hellberg, R.D. Thomas, M. Larsson, J. Chem. Phys. **122**, 014302 (2005)
A.V. Phelps, $H_3^+ + H_2$ cross sections (unpublished report dated 19 August 2001) (private communication)
D.S. Pollock, G.B.I. Scott, L.F. Phillips, Geophys. Res. Lett. **20**, 727–729 (1993)
R. Protz, M. Maier, J. Chem. Phys. **73**, 5464–5467 (1980)
G. Quemener, B. Naduvalath, D.L. Huestis, Charge exchange and vibrational relaxation in collisions of H^+ with H_2(v). Quant. Chem. Calc. (2008, in progress)
D. Régo, R. Prangé, L. Ben Jaffel, J. Geophys. Res. **104**, 5939–5954 (1999)
B.A. Ridley, R. Atkinson, K.H. Welge, J. Chem. Phys. **58**, 3878–3880 (1973)
R.G. Roble, Energetics of the mesosphere and thermosphere, in *The Upper Mesosphere and Lower Thermosphere: A Review of Experiment and Theory*, R.M. Johnson, T.L. Killeen, eds., AGU Monograph **87**, 1–21 (1995)
B.R. Rowe, D.W. Fahey, F.C. Fehsenfeld, D.L. Albrighton, J. Chem. Phys. **73**, 194–205 (1980)
J. Rufus, G. Stark, P.L. Smith, J.C. Pickering, A.P. Thorne, J. Geophys. Res. **108**(E2) (2003). doi:10.1029/2002JE001931
D.W. Rusch, D.G. Torr, P.B. Hays, J.C.G. Walker, J. Geophys. Res. **82**(4), 719–722 (1977)
S.P. Sander, V.L. Orkin, M.J. Kurylo, D.M. Golden, R.E. Huie, C.E. Kolb, B.J. Finlayson-Pitts, M.J. Molina, R.R. Friedl, A.R. Ravishankara, G.K. Moortgat, H. Keller-Rudek, P.H. Pine, Chemical kinetics and photochemical data for use in atmospheric studies, evaluation number 15. JPL Publication 06-2 (Jet Propulsion Laboratory, California Institute of Technology, Pasadena, CA, November 20, 2006). http://jpldataeval.jpl.nasa.gov/
G.C. Schatz, M.J. Redmon, Chem. Phys. **58**, 195–201 (1981)
H.I. Schiff, The photolysis of CO_2 at 1470 Å. Final report on grant No. DA-ARO(D)-31-124-0507, McGill University, Montreal Canada, November 1965
G.B.I. Scott, D.S. Pollock, L.F. Phillips, J. Chem. Soc. Faraday Trans. **98**, 1183–1188 (1993)
M. Seidl, J. Kaa, M. Maier, Chem. Phys. **157**, 279–285 (1991)
R. Shakeshaft, Phys. Rev. A **18**, 1930–1934 (1978)
D.A. Shaw, D.M.P. Holland, M.A. Hayes, M.A. MacDonald, A. Hopkirk, S.M. McSweeney, Chem. Phys. **198**, 381–396 (1995)
D.E. Shemansky, X. Liu, J. Geophys. Res. **110**, A07307 (2005)
V.I. Shematovich, R.E. Johnson, Adv. Space Res. **27**, 1881–1888 (2001)
V.I. Shematovich, R.E. Johnson, J.F. Cooper, M.C. Wong, Icarus **173**, 480–498 (2005)
G.M. Shved, L.E. Khvorostovskaya, I.Yu. Potekhin, A.I. Dem'yanikov, A.A. Kutepov, V.I. Fomichev, Izvestiya. Atmos. Ocean. Phys. **27**, 295–299 (1991)
J.P. Singh, D.W. Setser, J. Phys. Chem. **89**, 5353–5358 (1985)
G.G. Sivjee, J. Geophys. Res. **88**(A1), 435–441 (1983)
G.G. Sivjee, Planet. Space Sci. **39**, 777–784 (1991)
I.R. Slagle, D. Gutman, J.W. Davies, M.J. Pilling, J. Phys. Chem. **92**, 2455–2462 (1988)
T.G. Slanger, G. Black, J. Chem. Phys. **54**, 1889–1898 (1971)
T.G. Slanger, G. Black, J. Chem. Phys. **68**, 1844–1949 (1978)
T.G. Slanger, P.C. Cosby, Ground-based optical signatures of solar storms interacting with the ionosphere. SRI International proposal PYU 07-016, submitted in response to solicitation NSF 07-520 (January 2007)

T.G. Slanger, R.L. Sharpless, G. Black, S.V. Filseth, J. Chem. Phys. **61**, 5022–5027 (1974)
T.G. Slanger, R.L. Sharpless, G. Black, J. Chem. Phys. **67**, 5317–5323 (1977)
T.G. Slanger, P.C. Cosby, D.L. Huestis, R.R. Meier, J. Geophys. Res. **109**, A10309 (2004)
T.G. Slanger, D.L. Huestis, P.C. Cosby, N.J. Chanover, T.A. Bida, Icarus **182**, 1–9 (2006)
T.G. Slanger, K.S. Kalogerakis, L.C. Lee, Excited state photofragment yields from CO_2 and H_2O (2008a, experiments in progress)
T.G. Slanger et al., Photoemission phenomena in the solar system. Space Sci. Rev. (2008b, this issue). Chapter 7
F.J. Smith, Proc. Phys. Soc. **92**, 866–870 (1967)
G.P. Smith, Chem. Phys. Lett. **376**, 381–388 (2003)
D.L. Smith, J.H. Futrell, Chem. Phys. Lett. **40**, 229–232 (1976)
N. Smith, F. Raulin, J. Geophys. Res. **104**(E1), 1873–1876 (1999)
G.P. Smith, R. Robertson, Chem. Phys. Lett. **458**, 6–10 (2008). doi:10.1016/j.cplett.2008.04.074
P.L. Smith, K. Yoshino, W.H. Parkinson, K. Ito, G. Stark, J. Geophys. Res. **96**(E2), 17,529–17,533 (1991)
N.S. Smith, Y. Bénilan, P. Bruston, Planet. Space Sci. **46**, 1215–1220 (1998)
J.A. Spirko, J.J. Zirbel, A.P. Hickman, J. Phys. B **36**, 1645–1662 (2003)
J.R. Stallcop, H. Partridge, E. Levin, J. Chem. Phys. **95**, 6429–6439 (1991)
P.C. Stancil, D.R. Schultz, M. Kimura, J.-P. Gu, G. Hirsch, R.J. Buenker, Astron. Astrophys. Suppl. Ser. **140**, 225–236 (1999)
G. Stark, P.L. Smith, J. Rufus, A.P. Thorne, J.C. Pickering, G. Cox, J. Geophys. Res. **104**(E4), 16,585–16,590 (1999)
G. Stark, K. Yoshino, P.L. Smith, K. Ito, J. Quant. Spectrosc. Radiat. Transf. **103**, 67–73 (2007)
A.W. Stephan, R.R. Meier, K.F. Dymond, S.A. Budzien, R.P. McCoy, J. Geophys. Res. **108**(A1), 1034 (2003)
A.I.F. Stewart, M.J. Alexander, R.R. Meier, J.J. Paxton, S.W. Bougher, C.G. Fesen, J. Geophys. Res. **97**, 91–102 (1992)
L.J. Stief, W.A. Payne, R.B. Klemm, J. Chem. Phys. **62**, 4000–4008 (1975)
D.F. Strobel, M.E. Summers, Triton's upper atmosphere and ionosphere, in *Neptune and Triton*, ed. by D.P. Cruikshank (U. Arizona Press, Tucscon, 1995), pp. 1107–1148
T. Terao, R.A. Back, J. Phys. Chem. **73**, 3884–3890 (1969)
L.P. Theard, W.T. Huntress Jr., J. Chem. Phys. **60**, 2840–2848 (1974)
J.J. Thompson, Philos. Mag. **21**, 225 (1911)
A.P. Thorne, C.J. Harris, I. Wynne-Jones, R.C.M. Learner, G. Cox, J. Phys. E Sci. Instrum. **20**, 54–60 (1987)
A.P. Thorne, U. Litzen, S.E. Johannson, *Spectrophysics: Principles and Applications* (Springer, Berlin, 1999)
M.R. Torr, P.G. Richards, D.G. Torr, J. Geophys. Res. **85**, 6819–6826 (1980)
L.M. Trafton, T.R. Geballe, S. Miller, J. Tennyson, G.E. Ballester, Astrophys. J. **405**, 761–766 (1993)
C. Tully, R.E. Johnson, Planet. Space Sci. **49**, 533–537 (2001)
C. Tully, R.E. Johnson, J. Chem. Phys. **117** 6556–6561 (2002)
C. Tully, R.E. Johnson, J. Chem. Phys. **119**(E) 10452–10453 (2003)
G.L. Tyler et al., Science **246**, 1466–1473 (1989)
D. Uy, M. Cordonnier, T. Oka, Phys. Rev. Lett. **78**, 3844–3846 (1997)
V. Vuitton, R.V. Yelle, M.J. McEwan, Icarus **191**, 722–742 (2007)
J.H. Waite Jr., W.S. Lewis, G.R. Gladstone, T.E. Cravens, A.N. Maurellis, P. Drossart, J.E.P. Connerney, S. Miller, H.A. Lam, Adv. Space Res. **20**, 243–252 (1997)
J.C.G. Walker, D.G. Torr, P.B. Hays, D.W. Rusch, K. Docken, G. Victor, M. Oppenheimer, J. Geophys. Res. **82**(4), 719–722 (1975)
C.W. Walter, P.C. Cosby, J.R. Peterson, J. Chem. Phys. **98**, 2860 (1993)
J.-H. Wang, K. Liu, Z. Min, H. Su, R. Bersohn, J. Preses, J. Larese, J. Chem. Phys. **113**, 4146–4152 (2000)
K. Watanabe, M. Zelikoff, E.C.Y. Inn, Absorption coefficients of several atmospheric gases. Air Force Cambridge Research Labs, Hanscom AFB, MA (1953) [DTIC AD0019700]
K.H. Welge, R. Gilpin, J. Chem. Phys. **54**, 4224–4227 (1971)
E.P. Wigner, Phys. Rev. **73**, 1002–1009 (1948)
E. Wild, H. Klingshirn, B. Faltermeier, M. Maier, Chem. Phys Lett. **93**, 490–494 (1982)
E. Wild, H. Klingshirn, M. Maier, J. Photochem. **25**, 131–143 (1984)
J. Wildt, G. Bednarek, E.H. Fink, R.P. Wayne, Chem. Phys. **122**, 463–470 (1988)
O. Witasse et al., Ionospheres. Space Sci. Rev. (2008, this issue). Chapter 6
A.B. Wittkower, G. Ryding, H.B. Gilbody, Proc. Phys. Soc. **89**, 541–546 (1966)
A.-S. Wong, A.Y.T. Lee, Y.L. Yung, J.M. Ajello, Astrophys. J. **534**, L215–L217 (2000)
A.-S. Wong, Y.L. Yung, A.J. Friedson, Geophys. Res. Lett. **30**, 1447 (2003). doi:10.1029/2002GL016661
C.Y.R. Wu, B.W. Yang, F.Z. Chen, D.L. Judge, J. Caldwell, L.M. Trafton, Icarus **145**, 289–296 (2000)
C.Y.R. Wu, F.Z. Chen, D.L. Judge, J. Geophys. Res. **106**(E4), 7629–7636 (2001)
C.Y.R. Wu, F.Z. Chen, D.L. Judge, J. Geophys. Res. **109**, E07S15 (2004)

Z. Xie, B.J. Braams, J.M. Bowman, J. Chem. Phys. **122**, 224307 (2005)
R.V. Yelle, N. Borggren, V. de la Haye, W.T. Kasprzak, H.B. Niemann, I. Müller-Wodard, J.H. Waite, Icarus **182**, 567–675 (2006)
K. Yoshino, J.R. Esmond, Y. Sun, W.H. Parkinson, K. Ito, T. Matsui, J. Quant. Spectrosc. Radiat. Transf. **55**, 53 (1996)
Y.L. Yung, W.B. DeMore, *Photochemistry of Planetary Atmospheres* (Oxford University Press, New York, 1999)
Y.L. Yung, M.B. McElroy, Icarus **30**, 97–103 (1977)
O. Zatsarinny, S.S. Tayal, J. Phys. B **35**, 241–253 (2002)
M.H.G. Zhang, J.G. Luhmann, A.F. Nagy, J.R. Spreiter, S.S. Stahara, J. Geophys. Res. **98**(E2), 311–3318 (1993)
Y.-F. Zhu, R.J. Gordon, J. Chem. Phys. **92**, 2897–2901 (1990)
J.F. Ziegler, SRIM – The stopping and range of ions in matter (2008). http://www.srim.org/